Technology Development for Iron and Cobalt Fischer-Tropsch Catalysts

Quarterly Report

July 1, 2001 to September 30, 2001

Burtron H. Davis

Enrique Iglesia (UC/B Subcontract)

University of Kentucky Research Foundation

201 Kinkead Hall

Lexington, KY 40506

University of California-Berkeley (Subcontract)

Laboratory for the Science and Application of Catalysis

Department of Chemical Engineering

University of California at Berkeley

Berkeley, CA 94720

Abstract

<u>CAER</u>

The deactivation of a promoted 0.2%Re-15%Co/Al$_2$O$_3$ catalyst during Fischer-Tropsch synthesis in a CSTR was investigated. A novel method was utilized to isolate samples of catalyst from the reactor during the course of the reactor run, so that the catalyst was cooled in the solid wax for XAFS investigation. Results showed, as suggested in an earlier study of spent noble metal promoted catalysts, that the deactivation involves two processes. EXAFS strongly indicates significant cluster growth with time on-stream by a sintering process as a major component to the deactivation. However, in line with our previous investigation, XANES of the most heavily deactivated samples indicates that a fraction of Co species underwent a phase transformation to a phase resembling that of CoAl$_2$O$_4$. Addition of metal promoters to achieve reduction of Co species in interaction with the support results in higher initial activity by the formation of additional active sites. However, these additional Co metal clusters are unstable and are likely the cause of the higher initial deactivation rates of these catalysts during Fischer-Tropsch synthesis.

Preliminary experiments were successful in verifying the liquid displacement hold-up measurement techniques used during SBCR pilot plant runs. Gas hold-up results obtained using this method compared favorably to direct gas hold-up measurements using differential pressure transducers located axially along the bubble column. Generally, gas hold-up was proportional to the superficial velocity within the reactor. Over a pressure range of 25-100 psig, both methods of measurement indicated that gas hold-up was relatively independent of pressure.

<u>UC/B</u>

Most of the efforts during this reporting period were focused on the preparation of a final report and manuscripts covering the work done the past several months. A new transient

experimental setup that was developed during the previous quarter in order to perform transient

isotopic switch experiments, was tested and the surface capacity of one Fe-Zn-Cu-K sample was

measured by it. Switching experiments were also carried out on the Co-FT unit under typical

reaction conditions in order to estimate the number of active sites on the catalyst during the

reaction. The experimental technique for collecting data and analyzing them was modified in

order to take into account active sites only.

Table of Contents

4

Executive Summary

CAER

The deactivation of a promoted 0.2%Re-15%Co/Al$_2$O$_3$ catalyst in a CSTR was

investigated. A novel method of isolating samples of catalyst directly from the reactor during

the course of reaction testing in solid wax for XAFS investigation was demonstrated. Results

showed, as suggested in an earlier study of spent noble metal promoted catalysts, that the

deactivation likely involves two processes. First, EXAFS of samples with time on-stream

strongly indicates significant cluster growth by a sintering process as a major component to the

deactivation. However, in line with our previous investigation, XANES of the most heavily

deactivated samples indicates that a fraction of Co species underwent a phase transformation to a

phase resembling that of CoAl$_2$O$_4$. Addition of metal promoters to achieve reduction of Co

species in interaction with the support results in unstable Co metal clusters, which are likely the

cause of the higher initial deactivation rates of these catalysts during Fischer-Tropsch synthesis.

In this report we describe cold model bubble column operating experiences using a two-

phase water/argon system to simulate flow dynamics in the CAER's SBCR pilot plant. The

objectives of the cold model study were to: 1) develop correlations for gas hold-up as a function

of pressure and superficial velocity; 2) estimate liquid turnover rates as a function of superficial

gas velocity in the column; and 3) determine the extent of slugging within the bubble column.

In addition, transient tests were performed to simulate process upsets experienced in the SBCR

pilot plant system.

Preliminary experiments were completed to verify the hold-up measurement techniques

based on liquid displacement used during SBCR pilot plant runs. Additionally, gas hold-up was

estimated using differential pressure transducers located axially along the bubble column and

riser tube sections. This method, over a pressure range of 0-100 psig, compared favorably to the liquid displacement method used online with the SBCR.

A turbine flow meter was installed in the downcomer line of the cold model in order to measure the liquid recirculation rate; however, sporadic liquid flow in this location complicated accurate rate measurements with this instrument type. The maximum theoretical liquid recirculation rate was estimated using a mechanical energy balance along the surface of the liquid in the overhead separator to the exit of the downcomer tube within the bubble column. Another liquid rate estimation method was developed using the calculated liquid hold-up measurement in the riser section and actual volumetric gas rate exiting the column.

UC/B

Most of the current reporting period was utilized in order to prepare a final report that discusses the accomplishments of this project over the last three years in detail. In particular, the characterization of the Fe_xC active sites, the effect of promoters such as Zn, Cu, K and Ru and the structure and active site density as well as on the FTS rates and selectivities have also been reported.

In this reporting period, the new transient experimental setup designed to calculate the active site density on Fe catalysts during FTS reactions was tested. The mixing behavior of the micro fluid reactor was also measured. Additionally, the time resolution of the gas inlet manifold/micro fluidized reactor was determined by frequency response analysis. The reactor can be considered as a CSTR above a flow rate of 50 ml/min and the time resolution is around 5 sec.

Surface capacity of adsorbed CO at working condition was measured for the Fe-Zn-K_8-Cu_4 catalyst sample by ^{12}CO/^{13}CO isotopic switch. The amount of adsorbed CO was determined to be 12.7 mmol/g atom Fe at 523 K. The conversion was 8%. The background capacity was measured by loading graphite in the reactor.

A manuscript describing the effect of water on the FTS rates and selectivities and its correlation with the active carbon coverage on Co-FTS catalysts was also prepared. Our results show that the rate enhancement by water on Co catalysts is not reflected by a corresponding increase in the active carbon coverage.

Task 1. Iron Catalyst Preparation

The objective of this task is to produce robust intermediate- and high-α catalysts.

No scheduled or further activity to report.

Task 2. Catalyst Testing

The objective of this task is to obtain catalyst performance on the catalysts prepared in Task 1.

No scheduled or further activity to report.

Task 3. Catalyst Characterization

The objective of this task is to obtain characterization data of the prepared catalysts using routine and selected techniques.

A. EXAFS Characterization of Used 0.2% Re - 15% Co/Al$_2$O$_3$ Catalysts

ABSTRACT

The deactivation of a promoted 0.2%Re-15%Co/Al$_2$O$_3$ catalyst during Fischer-Tropsch synthesis in a CSTR was investigated. A novel method was utilized to isolate samples of catalyst from the reactor during the course of the reactor run, so that the catalyst was cooled in the solid wax for XAFS investigation. Results showed, as suggested in an earlier study of spent noble metal promoted catalysts, that the deactivation involves two processes. EXAFS strongly indicates significant cluster growth with time on-stream by a sintering process as a major component to the deactivation. However, in line with our previous investigation, XANES of the most heavily deactivated samples indicates that a fraction of Co species underwent a phase transformation to a phase resembling that of CoAl$_2$O$_4$. Addition of metal promoters to achieve reduction of Co species in interaction with the support results in higher initial activity by the formation of additional active sites. However, these additional Co metal clusters are unstable

8

and are likely the cause of the higher initial deactivation rates of these catalysts during Fischer-Tropsch synthesis.

INTRODUCTION

Extended X-ray absorption fine structure (EXAFS) spectroscopy is a powerful tool in that it provides information on the local structure surrounding the type of atom under investigation. For example, the average coordination information can be obtained [1,2], which is very useful for obtaining information regarding the dispersion of fresh catalysts, as well as the changes in the cluster size of supported metal catalysts during the course of a reaction. In some cases, information regarding cluster morphology can also be predicted [1,2]. It is important to note that, although EXAFS provides information regarding the local structure surrounding an atom, including atom type, degree of coordination, radial distances, and disorder parameters, the method represents an average over all the clusters present on the catalyst. XANES, on the other hand, can provide qualitative information on the oxidation states of species present on supported metal catalysts [3].

Re addition was found to catalyze the reduction of the very well dispersed Co species in interaction with the support, thereby increasing the number of Co active metal sites for reaction. The reduction of these additional species showed a slight lowering of the average cluster size in H_2 chemisorption/pulse reoxidation measurements in reference to the unpromoted catalyst, demonstrating that they were more highly dispersed. However, while the initial catalytic activity by addition of Re promoter was increased relative to the unpromoted catalyst, the deactivation rate was higher. Therefore, one focus of this paper was to use XAFS techniques to provide information on the nature of the deactivation of these small cobalt metal clusters, which were reduced in the presence of the Re, during the course of Fischer Tropsch synthesis. In order to

carry out these experiments, we developed a method of isolating catalyst samples in the solid wax directly from the CSTR during the course of reaction testing.

EXPERIMENTAL

Catalyst Preparation

Condea Vista Catalox (high purity γ-alumina, 100-200 mesh, 200 m^2/g) was the support for the cobalt FTS catalysts. To obtain a cobalt loading of 15%, a three step incipient wetness impregnation (IWI) was used with intermediate drying steps at 353 K in a rotary evaporator following each impregnation. The promoter was added after the third drying step by IWI of an aqueous solution of rhenium oxide salt. The catalyst was dried and then calcined under air flow at 673 K for 4 hrs following promoter addition. The cobalt loading was verified by ICP analysis.

Temperature Programmed Reduction

Temperature programmed reduction (TPR) profiles of catalysts were recorded using a Zeton Altamira AMI-200 unit. Calcined fresh samples were first purged in flowing inert gas to remove traces of water. TPR was performed using a 10% H_2/Ar mixture referenced to Ar at a flowrate of 30 ccm. The sample was heated from 323 K to 1073 K using a heating ramp of 10 K/min. Results are shown in Figure 1.

H_2 Chemisorption by TPD and % Reducibility by Reoxidation

The amount of chemisorbed hydrogen was measured using the Zeton Altamira AMI-200 unit, which incorporates a thermal conductivity detector (TCD). The sample weight was always 0.220 g. The catalyst was activated using hydrogen at 623K for 10 hrs and cooled under flowing hydrogen to 373 K. The sample was held at 373 K under flowing argon to prevent adsorption of physisorbed and weakly bound species, prior to increasing the temperature slowly to the reduction temperature. At that temperature, the catalyst was held under flowing argon to desorb

the remaining chemisorbed hydrogen until the TCD signal returned to the baseline. The TPD

spectrum was integrated and the number of moles of desorbed hydrogen determined by

comparing to the areas of calibration pulses of hydrogen in argon. Prior to experiments, the

sample loop was calibrated with pulses of N_2 in a helium flow and compared against a

calibration line produced from using gas tight syringe injections of N_2 into a helium flow.

After TPD of H_2, the sample was reoxidized [4] at the activation temperature by pulses of

pure O_2 in helium carrier referenced to helium gas. After oxidation of the cobalt metal clusters

(where the entire O_2 pulse was observed by the TCD), the number of moles of O_2 consumed was

determined, and the percentage reduction was calculated assuming that Co^0 reoxidized to Co_3O_4.

In order to estimate the average cluster size, the percentage reduction was included in the

dispersion calculation as follows, assuming a H:Co stoichiometric ratio of 1:1, as reported

previously [5].

$$\%D = (\text{number of surface } Co^0 \text{ atoms})/(\text{number of total } Co^0 \text{ atoms})$$

$$\%D = (\text{number of surface } Co^0 \text{ atoms})/[(\text{number of total Co atoms})(\text{percentage reduction})]$$

In Table 1, the dispersions and cluster sizes are first reported as uncorrected, which

assumes that all of the cobalt is reduced. Then, the percentage reduction is included in the

calculation and the corrected dispersion and cobalt cluster size is reported. This demonstrates

the importance of considering the fraction of cobalt species reduced in any estimate of dispersion

based on chemisorption measurements.

XAFS

Used catalyst samples were obtained from the continuously stirred tank reactor (CSTR)

at different points of catalyst deactivation with time onstream. The catalyst particles, well-mixed

with the reactor wax, were removed by a pressure letdown valve to a collection trap under inert

gas. The wax was allowed to cool, sealing the catalyst in the solid wax matrix for EXAFS analysis.

XAFS spectra at the Co K edge were obtained at the National Synchrotron Light Source (NSLS) at Brookhaven National Laboratory (BNL) in Upton, New York at beamline X18b. The X-rays were tuned by a Si(111) double crystal monochromator, which was detuned slightly to prevent glitches from harmonics. The used catalyst in the wax was pressed into a disk and loaded into a XAFS cell, which was cooled to liquid nitrogen temperatures prior to scanning under flowing helium. XAFS spectra of the Co foil, Co_3O_4, CoO, and $CoAl_2O_4$ were also measured. Several scans of the catalyst samples were obtained and the spectra averaged to improve the signal to noise ratio.

XANES and EXAFS spectra were first background corrected and normalized by dividing by the height of the edge jump to account for the concentration of Co atoms in the sample. For EXAFS spectra, appropriate splines were used to remove the background based on the Nyquist criteria [6]. The Chi function in energy space was extracted and converted to k space and weighted with either k^0 or k^3 weighting for examination of the changes in coordination number of the different Z scatterers. To obtain information on Co-Co coordination and therefore, changes in the cluster size, the k^3-weighted spectrum was transformed from k space to r space to obtain the radial distribution function. The EXAFS spectrum for the first Co-Co coordination shell was isolated and the inverse Fourier Transform was conducted. Fitting of the spectra in k space was carried out using FEFFIT [4]. Theoretical EXAFS were generated using FEFF [7] using model Co metal crystal parameters generated by Atoms [8]. In order to use coordination number as a fitting parameter, S_0^2 was first obtained from analysis of the Co foil assuming a fixed coordination number N_1 of 12 for the first shell. The other fitting parameters utilized by FEFFIT included the overall E_0 shift e_0 applied to each path, *delr* to account for lattice expansion, and

12

sigma², which is based on a correlated Debye model used to approximate the mean square

disorder in the path length of each path [8].

RESULTS AND DISCUSSION

Figure 2 shows the points during the initial deactivation period of the catalyst where the

catalyst was removed. Figure 3 shows the k^0 and k^3-weighted radial distribution functions for the

used catalyst withdrawn from the reactor at 1800 hours onstream and a comparison against those

of the standards. The aim of this part of the investigation was to determine whether the small Co

metal clusters showed signs of reoxidation, as had been suggested in earlier reports [9,10], or

whether the main cause of the deactivation was by growth of the Co metal cluster by a sintering

mechanism, leading to a loss of surface sites.

Figure 3 displays the normalized XANES spectra of the catalyst samples removed at

1800 and 2135 hours onstream with a comparison against those of the reference compounds,

including the Co metal foil and CoO, Co_3O_4, and $CoAl_2O_4$ standards. Interestingly, as noted

previously in other spent catalysts [11], the XANES reveals two contributions, a strong

contribution of the reduced Co metal and three small peaks which match very well the positions

of the $CoAl_2O_4$ standard. The positions are more pronounced when one considers the derivative

spectra. These suggest the possibility that a small fraction of the clusters may have undergone a

phase transformation to an oxidized state. In comparison with our earlier study [11], the extent

of formation of this oxidized phase is less pronounced than the unpromoted catalyst, indicating

that Re promoter may play a role in suppressing its formation.

Both the k^0 and k^3-weighted radial distribution functions displayed in Figure 4 for the

used catalyst withdrawn from the reactor at 1800 hours onstream strongly resemble the

corresponding spectra of the Co foil. Surprisingly, even in the k^0-weighted spectra, there is not a

peak present at low R between 1 and 2 Angstroms that suggests an increase in the Co-O

coordination, in comparison with the references where the Co is in an oxidized state. Also, a comparison in k^3 of the CoO, Co_3O_4, and $CoAl_2O_4$ standards show the Co-Co distances are shifted to higher R, as expected, in comparison with the Co foil. However, there is no indication of a contribution from Co-Co distance at these higher R in the used catalyst sample, rather only the Co-Co distance which matched closely that found in the Co metal foil. Therefore, this suggests that if there is deactivation due to reoxidation, it is either likely limited to the surface of the catalyst or a surface phase, unable to be viewed by EXAFS, or the reoxidation is part of a dynamic oxidation/reduction cycle. That is, the EXAFS results suggest that the small Co metal clusters do not sustain a bulk reoxidized CoO or Co_3O_4 phase under the normal partial pressures of H_2O encountered in the Fischer Tropsch reactor in the presence of the reducing syngas.

Figure 5 shows the EXAFS data $Chi(k)*k^3$ v. k, the Fourier transform magnitude in r-space, and the first shell inverse transforms for Co metal and catalysts. The inverse transform is the solid line, while the plotted points indicate the fitting obtained from FEFFIT. It is clear by the augmentation of the intensity of the envelope in k-space and by the growth in the Fourier transform peak for Co-Co coordination, that the average metal cluster size has experienced an increase in size with time onstream in the CSTR. Table 2 shows the direct parameters obtained from FEFFIT analysis with their corresponding uncertainties.

Clearly, a substantial increase in Co-Co coordination as cobalt metallic phase is evident during the initial stages of the deactivation period, with a leveling off achieved at approximately 1800 hours of time onstream. This time also correlates very well with the greatest degree of deactivation in the CO conversion, as shown in Figure 2. Therefore, one cannot rule out a sintering mechanism as the main reason for the catalyst deactivation. Certainly, there is an additional fraction of Co metal reduced by addition of Re promoter as shown by the shift in reduction peaks to lower temperature, as demonstrated in Figure 1. This leads to a higher

fraction of very small Co metal clusters at the onset of reaction testing. These may be the result of the reduction of a surface phase of Co containing atoms of the support in their structure, or the reduction of very tiny Co oxide clusters which interact with the support and deviate from bulklike Co metal behavior. In either case, their resulting reduction results in a fraction of very small cobalt metal clusters, which causes a lowering of the average cluster size, as demonstrated by H_2 chemisorption/pulse reoxidation measurements in Table 1, in reference to the unpromoted catalyst.

These clusters, therefore, will have a higher surface free energy than the clusters reduced at the same temperature on the unpromoted catalyst. Such unstable clusters, with a greater number of dangling bonds, may therefore be more susceptible to cluster growth, although the actual kinetics of the process is not yet well understood. On the basis of XPS evidence which indicated surface oxidation of small Co clusters under H_2O/syngas mixtures, it is possible that the sintering may be the result of a dynamic reoxidation/reduction cycle. Such cycles have been shown previously to result in metal cluster growth.

One should also consider the possibility that a fraction of the small metal clusters underwent a phase transformation to an oxidized state during reaction. XANES suggest the formation of a $CoAl_2O_4$-like phase, which may not be seen directly by EXAFS. Loss of small metal clusters to an oxidized phase would also result in an increase in the average Co metal cluster size, which would show increased Co-Co coordination in the metallic phase. However, if the oxidation was sustained, then one would also expect to see the appearance and growth of a Co-O peak as well as a contribution from a Co-Co coordination at higher R for an oxidized Co phase, especially after the extent of deactivation observed in Figure 2. The EXAFS results presented here as a function of time onstream suggest an increase in the Co cluster size only, most likely the result of a slow loss of surface sites by a sintering process. Finally, addition of

Re promoter does aid in reducing the Co species, thereby generating a greater number of initial active sites, improving the initial activity. However, the resulting catalyst also showed a higher initial rate of deactivation than the unpromoted catalyst, indicating that promoter addition alone does not guarantee a better catalyst from the standpoint of long-term stability.

CONCLUSIONS

The deactivation of a promoted $0.2\%Re-15\%Co/Al_2O_3$ catalyst in a CSTR was investigated. A novel method of isolating samples of catalyst directly from the reactor during the course of reaction testing in solid wax for XAFS investigation was demonstrated. Results showed, as suggested in an earlier study of spent noble metal promoted catalysts, that the deactivation likely involves two processes. First, EXAFS of samples with time onstream strongly indicates significant cluster growth by a sintering process as a major component to the deactivation. However, in line with our previous investigation, XANES of the most heavily deactivated samples indicates that a fraction of Co species underwent a phase transformation to a phase resembling that of $CoAl_2O_4$. Addition of metal promoters to achieve reduction of Co species in interaction with the support results in unstable Co metal clusters, which are likely the cause of the higher initial deactivation rates of these catalysts during Fischer-Tropsch synthesis.

REFERENCES

1. Greegor, R.B., and Lytle, F.W., J. Catal. 63 (1980) 476.

2. Jentys, A., PCCP 1 (1999) 4059.

3. Bart, J.C.J., Adv. in Catal. 34 (1986) 203.

4. Vada, S., Hoff, A., Adnanes, E., Schanke, D., and Holmen, A., Topics in Catal. 2 (1995) 155.

5. Jacobs, G., Das, T.K., Zhang, Y.-Q., Li, J., Racoillet, G., and Davis, B.H., Appl. Catal. A: General, submitted.

6. Newville, M., Automated Background Removal for XAFS Data (1997).

7. Newville, M., Using FEFF to model XAFS data (1998).

8. Ravel, B., EXAFS Analysis Using FEFF and FEFFIT, Workshop (June 27, 2001).

9. Schanke, D., Hilmen, A.M., Bergene, E., Kinnari, K., Rytter, E., Adnanes, E., and Holmen, A., Catal. Lett. 34 (1995) 269.

10. Hilmen, A.M., Schanke, D., Hanssen, K.F., and Holmen, A., Appl. Catal A: General 186 (1999) 169.

11. Jacobs, G., Zhang, Y.-Q., Das, T.K., Li, J., Patterson, P.M., and Davis, B., Stud. Surf. Sci. Catal. 139 (2001) 415.

Catalyst	μmol H₂ desorbed per g cat	Uncorr %D	Uncorr diam. (nm)	μmol O₂ pulsed per g cat	% Red	Corr %D	Corr diam. (nm)
15%Co/Al₂O₃	67	5.3	19.6	509	30	17.6	5.9
0.2%Re-15%Co/Al₂O₃	142	11.2	9.2	939	55	20.4	5.1
0.5%Re-15%Co/Al₂O₃	143	11.3	9.2	993	59	19.1	5.4
1.0%Re-15%Co/Al₂O₃	168	13.2	7.8	1187	70	18.9	5.5

Table 1

H_2 chemisorption (TPD) and pulse reoxidation results for Al_2O_3 (200 m^2/g) Supported catalysts, with and without Re promoter

Table 2								
Best-fit values for average coordination number (N_1) for the first Co-Co shell, shift in E_0, Debye-Waller factor (σ^2), lattice expansion (*delr*), and fractional misfit (*r*). Relative uncertainties are also displayed.								
Sample	N_1	ΔN_1	e_0	Δe_0	σ^2	$\Delta \sigma^2$	*delr*	$\Delta delr$	*r*-factor
355 hours	2.68	0.43	2.56	1.94	0.00359	0.00133	-0.0258	0.0120	0.115
665 hours	3.47	0.37	3.10	1.27	0.00422	0.00093	-0.0216	0.00808	0.045
980 hours	5.61	0.28	5.49	0.59	0.00389	0.00043	-0.0166	0.00375	0.018
1340 hours	6.50	0.32	7.21	0.57	0.00399	0.00043	-0.00673	0.00368	0.017
1800 hours	7.56	0.27	7.74	0.41	0.00455	0.00032	-0.00407	0.00268	0.0088
2135 hours	7.65	0.34	7.70	0.50	0.00500	0.00041	-0.00303	0.00339	0.013
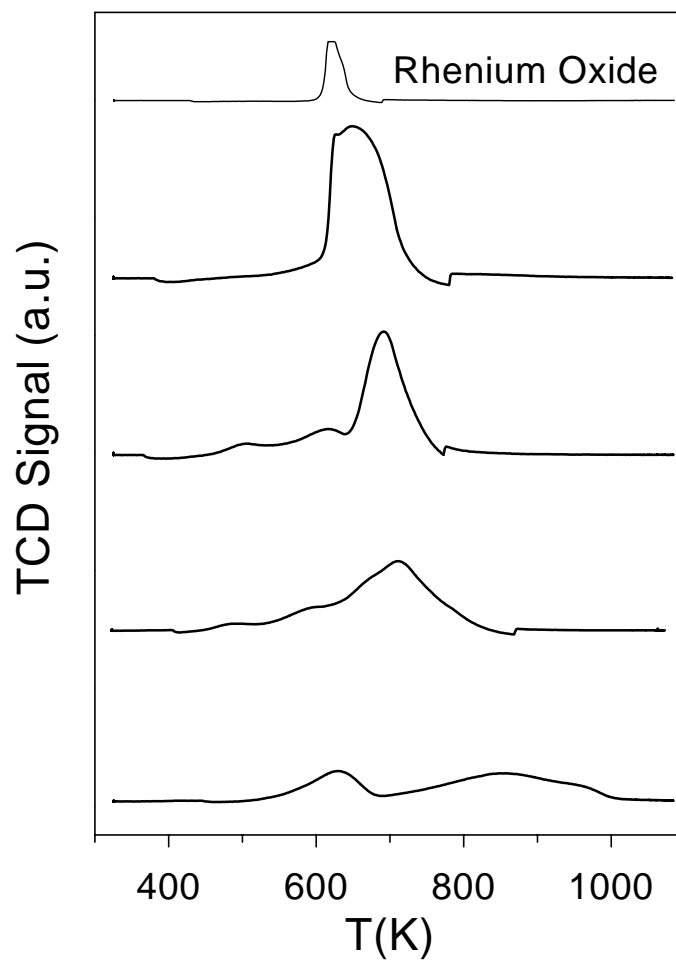
Figure 1.   Comparative TPR spectra of unpromoted (bottom) 15%Co/Al$_2$O$_3$ catalyst with those promoted with (moving up) 0.2%, 0.5%, and 1.0% Re. Top spectra is the reduction of Re$_2$O$_7$ precursor (unsupported).
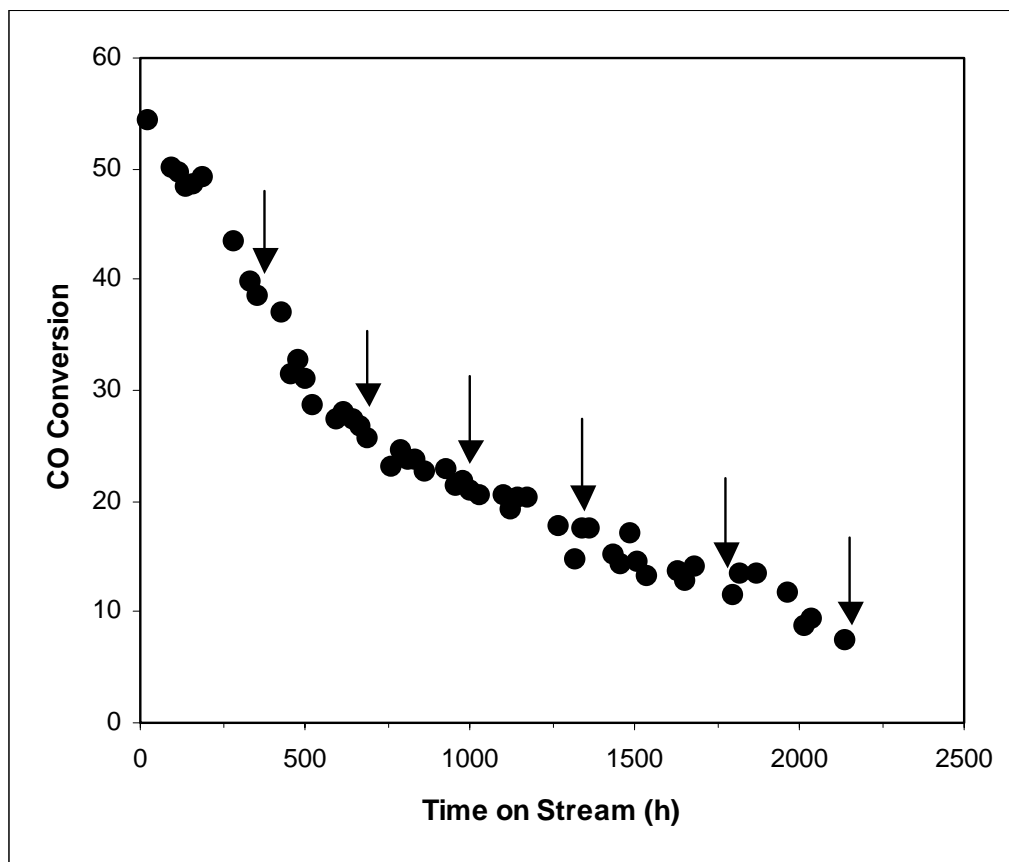
Figure 2.   Deactivation profile of the 0.2%Re-15%Co/Al$_2$O$_3$ catalyst. Reaction testing
conditions were as follows: 493K, 275 psig, 34 SL CO/g cat hr. Arrows indicate
points where wax-containing catalyst samples were removed from the reactor for
EXAFS analysis.
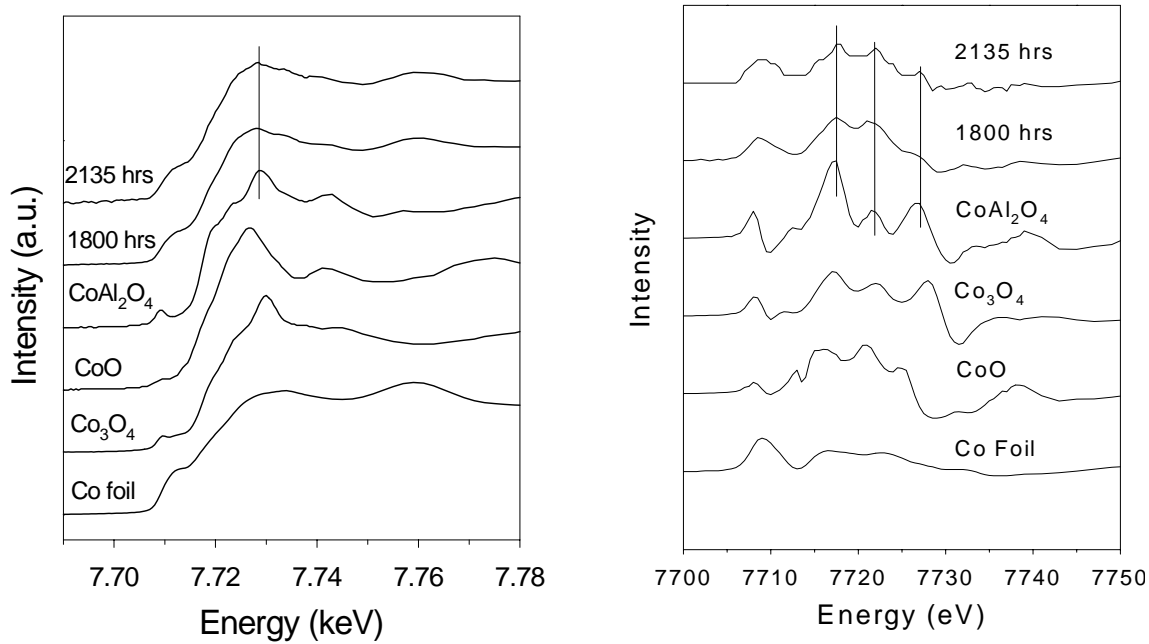
Figure 3.   Normalized Co *K*-edge XANES spectra (left) and XANES derivative spectra (right) of the used catalyst after deactivation time of 1800 hours and 2135 hours in the Fischer-Tropsch Synthesis CSTR reactor versus those of comparative standards, including Co metal foil, Co_3O_4, CoO, and $CoAl_2O_4$.
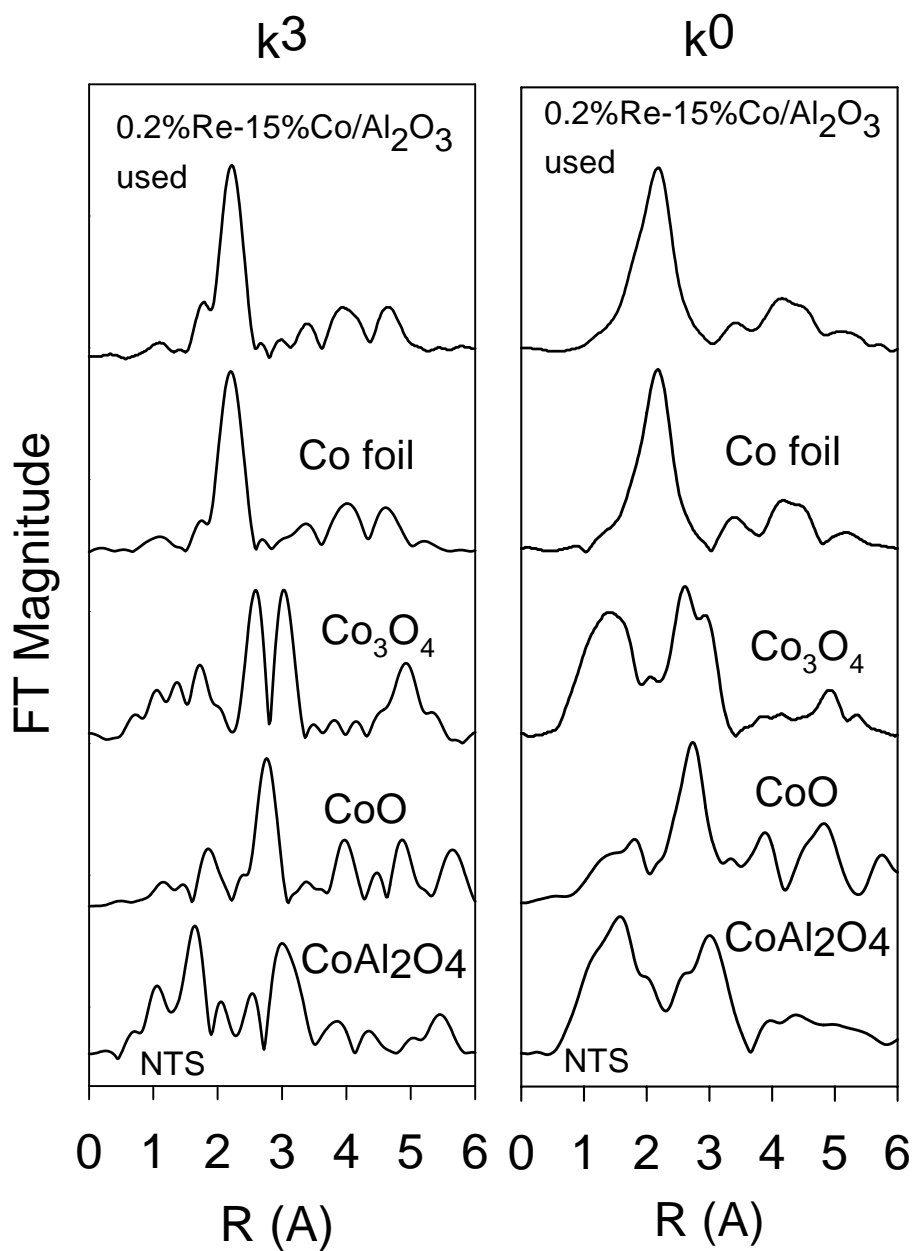
Figure 4. k^3 and k^0-weighted Fourier transform magnitudes of Co K-edge EXAFS spectra of the used catalyst after deactivation time of 1800 hours in the Fischer-Tropsch Synthesis CSTR reactor versus those of comparative standards, including Co metal foil, Co_3O_4, CoO, and $CoAl_2O_4$.
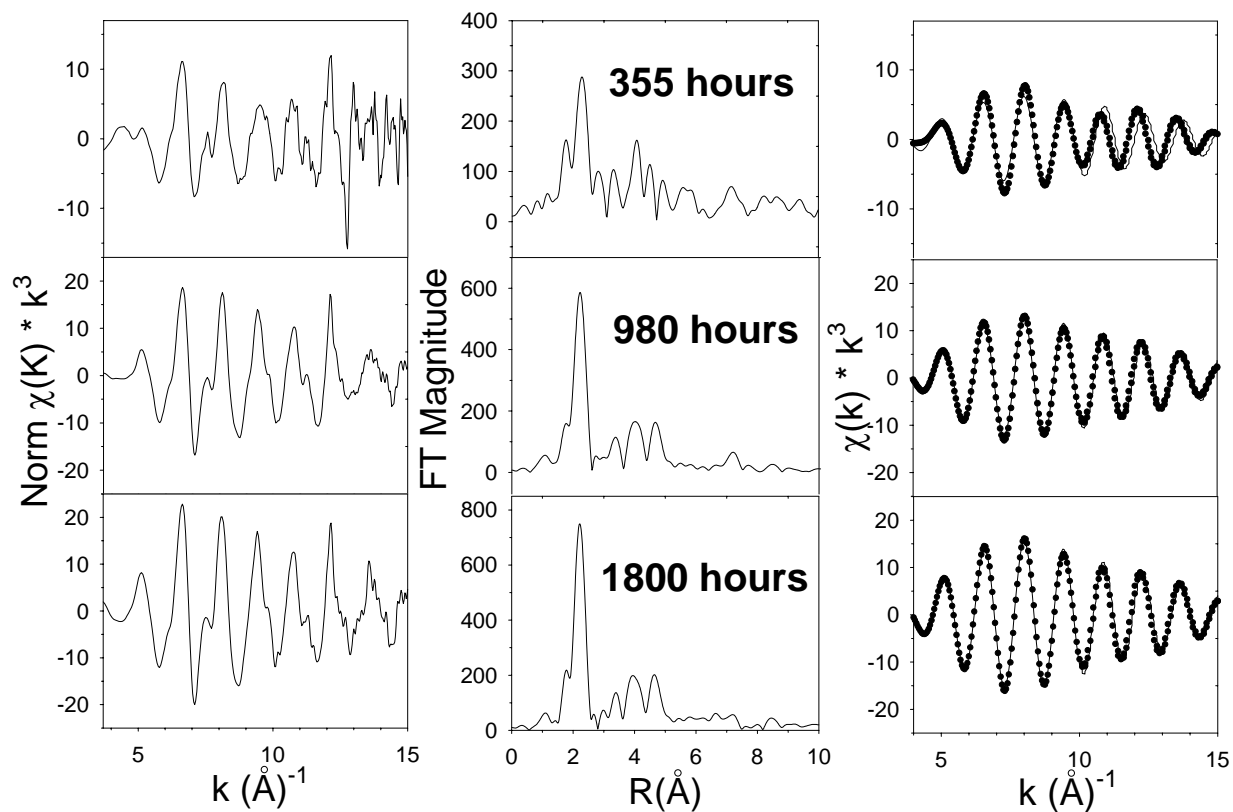
Figure 5. EXAFS results $\chi(k) \cdot k^3$ vs k, the Fourier transform magnitude, and first shell inverse transforms for used 0.2%Re-15%Co/γ-Al$_2$O$_3$ catalysts sampled during deactivation at 355, 980, and 1800 hours onstream, respectively. The solid lines represent the inverse transform, while the plotted points indicate the fit by FEFFIT.

Task 4. Wax/Catalyst Separation

The objective of this task is to develop techniques for the separation of catalysts from FT reactor slurries.

A. Cold Model Studies of the CAER Slurry Bubble Column Reactor.

Executive Summary

In this report we describe cold model bubble column operating experiences using a two-phase water/argon system to simulate flow dynamics in the CAER's SBCR pilot plant. The objectives of the cold model study were to: 1) develop correlations for gas hold-up as a function of pressure and superficial velocity; 2) estimate liquid turnover rates as a function of superficial gas velocity in the column; and 3) determine the extent of slugging within the bubble column. In addition, transient tests were performed to simulate process upsets experienced in the SBCR pilot plant system.

Preliminary experiments were completed to verify the hold-up measurement techniques based on liquid displacement used during SBCR pilot plant runs. Additionally, gas hold-up was estimated using differential pressure transducers located axially along the bubble column and riser tube sections. This method, over a pressure range of 0-100 psig, compared favorably to the liquid displacement method used online with the SBCR.

A turbine flow meter was installed in the downcomer line of the cold model in order to measure the liquid recirculation rate; however, sporadic liquid flow in this location complicated accurate rate measurements with this instrument type. The maximum theoretical liquid recirculation rate was estimated using a mechanical energy balance along the surface of the liquid in the overhead separator to the exit of the downcomer tube within the bubble column. Another liquid rate estimation method was developed using the calculated liquid hold-up measurement in the riser section and actual volumetric gas rate exiting the column.

Introduction

Gas hold-up or the fractional volume of gas occupying the bubble column or (e_g) is an

important factor for predicting both the flow and mass transfer dynamics within SBCR reactors.

As highlighted in previous reports [1,2,3,4], accurate estimation of e_g is crucial for determining

the gas space velocity in the CAER's unique SBCR design.

Slurry volume within the CAER pilot plant reactor was not directly measured. Instead,

only slurry occupying the overhead separator vessel was measured via a differential pressure

transmitter. The reactor vessel was always flooded with slurry/gas, provided a slurry level was

indicated in the overhead separator vessel; therefore, by knowing the gas holdup for any given

superficial velocity, the mass of slurry within the reactor could be estimated by difference. The

baseline liquid level in the overhead vessel was recorded without gas flowing through the reactor

(i.e., $U_g = 0$). Syngas flow was established at superficial velocities ranging from 0.7 to 3 cm/s.

The liquid level increase above the baseline level was effectively due to gas displaced in the

reactor vessel. Therefore, the displaced liquid volume divided by the reactor volume was equal

to e_g. The disadvantage of this liquid displacement method is that the gas supply must be

momentarily terminated during the run, thereby causing the catalyst particles to settle.

Gas hold-up is dependent on the bubble size and associated rise velocity behavior [5,6,7].

Many factors affect both of these parameters including: column diameter; gas sparger geometry

and orifice diameter; superficial velocity; existence of reactor internals such as heat transfer

surfaces; surface tension of the liquid; catalyst loading; and pressure. Numerous empirical

correlations exist for the prediction of the average gas hold-up in SBCR systems [5]. Most of

these correlations are valid for column diameters greater than 0.1 m and do not account for the

existence of reactor internals or liquid recycle.

26

The column diameter of the CAER's SBCR is relatively small (0.051 m) and contains an internal downcomer that provides for recycle of liquid. These unique features make the validity of the available gas hold-up correlations questionable. Liquid recycle in the CAER SBCR depends on the natural circulation driving force created by the gas bubbles in the column and riser sections. The magnitude of this liquid recycle had been estimated to be of the order 0 .1 to 1 min (in terms of the average liquid turnover rate).

Slurry back-mixing in the CAER's SBCR may be significantly reduced by the addition of the down-comer/dip-tube flow path; consequently, the gas and liquid phases likely exhibited more "plug-flow" behavior. It has been demonstrated that SBCR pilot plant yields a higher conversion than that of comparable CSTR tests [3]. Differences in conversion between the two reactor types may also be caused by the dissimilarity of heat and mass transfer phenomena related to the bubble dynamics and liquid turnover.

Although several successful pilot runs have been completed using the CAER's SBCR design, several uncertainties regarding the liquid turnover rate, bubble flow dynamics and gas hold-up exist. In order to address these engineering questions, a full-scale, transparent cold-flow model of the CAER's design was constructed. The main objective of the cold model study was to determine the relationship of gas hold-up and column pressure. Secondly, quantifying the liquid turnover rates as a function of superficial gas velocity in the column was a priority. The cold model would also allow the visualization of the extent of slugging within the bubble column. In addition, transient tests were performed to simulate process upsets experienced in the SBCR pilot plant system.

Experimental

The cold model apparatus, shown in schematically in Figure 1, was designed to be a 1:1 scale model of the CAER's SBCR [1,2,3,4]. In the current configuration, the cold model is

27

constructed of clear PVC Sch. 80 pipe and has a 5.08 cm diameter and a 2-m height with an effective reactor volume of 3.7 liters. Argon gas was passed continuously through the water-filled reactor and distributed by a sparger near the bottom of the reactor vessel. Gas and liquid exited the top of the reactor and passed through an overhead receiver vessel where the liquid was disengaged from the gas-phase. Argon gas exits the overhead vessel into a wet-test flow meter down stream of a back-pressure regulator. The cold model pressure could be safely regulated up to 150 psig.

A dip tube or down-comer connected the overhead vessel reservoir to the bottom of the reactor to allow internal liquid recycle via the natural convection loop. The fluidizing gas and liquid exited into a side port near the top of the column and entered a riser tube. The driving force for the recirculation flow was essentially the difference in density between the fluid column in the riser (liquid and gas) and that of the dip-tube (liquid only). The dip tube provided a downward flow path for the slurry without interfering with the upward flow of the turbulent syngas slurry mixture. Thus, to some degree, back mixing of the slurry phase and wall effects in the narrow reactor tube were minimized. A turbine-style flow meter with an effective range of 4-75 LPM (1-20 G.P.M.) was installed in the downcomer in an attempt to quantify the recirculation rate.

Gas hold-up in both the column and riser sections were measured via differential pressure transducers DP-1, DP-2, and DP-3 as depicted in Figure 1. The pressure legs of each differential transducer were flooded with water. Therefore, with column fully loaded with water, all of the DP cells registered zero. Once gas was introduced into the column and riser, the high pressure legs of each transducer remained flooded with water while the low pressure legs registered a decreased hydrostatic head due to the lower average density of the gas/water mixture in the column and riser sections.

Cold model experiments were conducted using superficial velocities from 1 to 8 cm/s with column pressures varying from 0 to 100 psig. Gas hold-up in the column and riser tube were calculated using the differential pressure transducers. Also, the column gas hold-up was calculated using the liquid displacement method as summarized in the previous section. During these tests, the axial position of slugging onset was recorded.

RESULTS

Gas Hold-up Measurements

The total differential pressure gradient along the column measured by the lower (DP_1) and upper (DP_2) pressure transducers was defined by the following equation:

$$- \frac{\Delta P}{\Delta h_{column}} \approx \frac{DP_1 + DP_2}{h_{ref} - (h_1 + h_2)} \approx (\varepsilon_s \, \rho_s + \varepsilon_L \, \rho_L) \, g \qquad (1)$$

In Equation (1), the frictional losses and the contribution of the gas phase hydrostatic head have been neglected. In a three-phase system, the volume fraction of each phase must follow the relation:

$$\varepsilon_{gc} + \varepsilon_{Lc} + \varepsilon_{sc} = 1 \qquad (2)$$

In the case of the cold model experiments only the liquid and gas phases (deionized water and argon gas) were present, therefore, $e_s = 0$. Thus, solving equations (1) and (2) for the gas hold-up yielded the following:

$$\varepsilon_{gc} = 1 - \frac{DP_1 + DP_2}{g\,\rho_L\,(h_1 + h_2)} \tag{3}$$

Likewise, an expression for the gas hold-up in the riser tube was developed:

$$\varepsilon_{gr} = 1 - \frac{DP_3}{g\,\rho_L\,h_3} \tag{4}$$

Results from the gas-hold-up tests for column pressures of 0,25,50,75 and 100 psig are displayed in Figures 2,3,4,5 and 6, respectively. In general, the liquid displacement method of measuring gas-hold in the column was in agreement with that of the differential pressure method. The liquid displacement method involved more opportunities for error since the change in slurry level was manually recorded from a ruler attached to the overhead vessel. This measurement error was compounded by the continually fluctuating liquid level.   The differential pressure measurement in the column and riser were taken by a computer data logging system and averaged over a 5 minute time interval. The largest difference between the two methods occurred during the 0 (Figure 2) and 50 (Figure 4) psig tests.

In all pressure tests, gas hold-up varied proportionally with U_g in a near linear fashion. The riser gas hold-up increased with Ug and tended to level off past 5 cm/s. During the entire range of tests, the riser flow was in the slugging regime.

Pressure Effects: Gas Hold-up and Column Slugging

Figure 7 shows the effect of pressure on the bubble column gas hold-up for superficial velocities of 3.0 and 5.0 cm/s using the argon/water two-phase system. The gas hold-up results for the 3.0 cm/s tests indicated an initial decrease with increasing pressure above atmospheric from 10% down to 6% by volume. Beyond a pressure of 25 psig, the gas hold-up in the column

30

remained relatively constant. For the 5.0 cm/s superficial velocity tests, the gas hold-up was nearly independent of pressure.

These results are consistent with experimental and modeling results of Krishna [8,9]. The range of superficial velocity in the cold model tests was low enough to keep the flow dynamics in the homogeneous regime (consisting of relatively small, uniform bubbles). Pressure effects tend to become more prevalent with larger bubbles encountered with larger diameter columns above the transition superficial velocity (> 5.0 cm/s).

The column position of initial bubble slugging versus pressure is displayed in Figure 8. At atmospheric pressure, the slug formation occurred just below 40% of the column length above the gas sparger for both 3.0 and 5.0 cm/s.   As the pressure was increased, slug formation tended to move up the column. However, at 5.0 cm/s, the axial position of slug formation remained unchanged.   Beyond 5.0 cm/s, the column flow dynamic began to fully transition into the slugging flow regime.

Estimation of Average Recirculation Rate

The turbine flow meter installed in the downcomer was not able to measure a consistent liquid recirculation rate. This was due in part to the sporadic liquid flow in this location , thereby complicating an accurate rate measurement. Another possibility was that the liquid recirculation rate was lower than initially anticipated. Therefore, the maximum theoretical liquid recirculation rate was estimated using a mechanical energy balance along the surface of the liquid in the overhead separator to the exit of the downcomer tube within the bubble column. Another liquid rate estimation method was developed using the calculated liquid hold-up measurement in the riser section and actual volumetric gas rate exiting the column.

Mechanical Energy Balance Method for Maximum Theoretical Flow

Ignoring friction energy losses and the absence of pump work, a simplified mechanical energy balance around the downcomer section of the cold model (as shown between elevations A & B in Figure 1) yields the basic form of the Bernoulli equation:

$$\frac{P_A - P_B}{\rho} + \frac{u_A + u_B}{2} + g\,(h_{diptube} - h_{ref}) = 0 \tag{5}$$

In this case, the reference elevation was assigned to the bottom portion of the diptube (point B). The top elevation considered was the surface of the liquid level in the overhead separator (point A).

P_A can be eliminated if we chose the reference pressure to be that at the liquid surface in the overhead separation vessel. Likewise, u_A, the velocity of the liquid surface is assumed to be zero since the bubble column is at steady-state with a constant liquid level . The reference elevation was arbitrarily set to the bottom of the bubble column such that $h_{ref} = 0$. Consequently, the Bernoulli equation for this application can simplified and rearranged to solve for u_B, the velocity of liquid exiting the diptube:

$$u_B = \sqrt{2\left(g\,h_{diptube} - \frac{P_B}{\rho_s}\right)} \tag{6}$$

P_B, the pressure outside the diptube exit, can be calculated from the hydrostatic pressure head of the gas and liquid flowing in the bubble column ($h_{\,column} = h_1 + h_2$) and the riser (h_r):

$$P_B = \rho_s\, g\, [\, (1 - \varepsilon_{gc})\, h_{column} \quad + \quad (1 - \varepsilon_{gr})\, h_r \,] \tag{7}$$

Thus, substituting Equation (7) into (6) becomes:

$$u_B = \sqrt{2\, g\, [\, h_{diptube} - (1 - \varepsilon_{gc})\, h_{column} \quad - \quad (1 - \varepsilon_{gr})\, h_r \,]} \tag{8}$$

Therefore, the maximum theoretical recirculation rate can be calculated knowing the cross-sectional area of the diptube:

$$Q_{recirc} = u_B\, A_{c_{diptube}} \;\rightarrow\; u_B\, \pi\, \frac{D^2_{diptube}}{4} \tag{9}$$

Inserting the appropriate constants and conversions for units of LPM, Equation (9) becomes:

$$Q_{recirc} = 8.42\, \sqrt{h_{diptube} - (1 - \varepsilon_{gc})\, h_{column} \quad - \quad (1 - \varepsilon_{gr})\, h_r} \quad (LPM) \tag{10}$$

Since h_r and h_{column} were fixed for each experiment, the only elevation measured was that of the liquid column in the diptube, $h_{diptube}$. Gas hold-up for the column and riser sections were calculated using Equations (3) and (4), respectively.

Figure 9 shows the calculated maximum recirculation rates for each of the pressures and superficial velocities tested. In general, the calculated maximum rate was a function of U_g. The highest recirculation rates were achieved for any given U_g at atmospheric pressure. The maximum theoretical liquid recirculation rate was estimated to be between 6-10 LPM (in terms of turnover rate, 0.5-0.3 min^{-1}, respectively) .

Liquid Recirculation Based on Liquid Hold-up in the Riser Tube

The riser section of the cold model was also constructed of clear PVC pipe so the hydrodynamics could be observed qualitatively. It was noticed that the narrow riser tube forced the gas/liquid flow into a slugging regime upon exiting the top of the column. As a result, very little liquid back mixing was observed in the riser.

If we can indeed assume that any liquid entering the riser exits into overhead vessel with the gas phase, then a simple relation using $\mathbf{e}_g$ and the actual gas flow exiting the column could be used to estimate the liquid recirculation rate. Neglecting the back-mixing within the riser, the following volumetric balance of the liquid phase around the riser tube is:

$$Q_L = (Q_g + Q_L) \; (1 - \varepsilon_{gr}) \tag{11}$$

Rearranging and solving for Q_L, Equation 11 becomes:

$$Q_L = Q_g \left(\frac{1 - \varepsilon_{gr}}{\varepsilon_{gr}} \right) \tag{12}$$

Equation (12) was applied to the experimental data for each of the pressures tested and plotted in Figure 10. The liquid recirculation rate was estimated to be between 2-6 LPM (in terms of turnover rate, 1.5-0.5 min^{-1}, respectively) and was dependent on superficial velocity and independent of column pressure for superficial velocities less than 5 cm/s. For Ug greater than 5 cm/s, the calculated recirculation rate decreased marginally with increasing pressure.

In Figure 11, the averaged recirculation rates results for all pressure tests from both the riser (Equation 12) and mechanical energy balance (Equation 10) methods were plotted. The error bars for each the constant U_g data points represent the standard deviation of averaged pressure test results. As expected, the mechanical energy balance method predicted

consistently higher recirculation rates than that of the riser flow method. This is reasonable since Equation (10) was based on the assumption that frictional losses were ignored. The data applied to the mechanical energy balance was reasonably fitted to a 2nd order polynomial with an R^2 of 0.9776. The experimental data fitted to Equation (12) resulted in a linear correlation of recirculation rate with U_g.

Conclusions and Summary

Preliminary experiments were successful in verifying the liquid displacement hold-up measurement techniques used during SBCR pilot plant runs. Gas hold-up results obtained using this method compared favorably to direct gas hold-up measurements using differential pressure transducers located axially along the bubble column. Generally, gas hold-up was proportional to the superficial velocity within the reactor. Over a pressure range of 25-100 psig, both methods of measurement indicated that gas hold-up was relatively independent of pressure.

A turbine flow meter installed in the downcomer line of the cold model was not able to measure consistent flow rates due to the sporadic nature of the liquid recirculation within the column. The maximum theoretical liquid recirculation rate was estimated to be between 6-10 LPM (in terms of turnover rate, 0.5-0.3 min^{-1}, respectively) using a mechanical energy balance along the surface of the liquid in the overhead separator to the exit of the downcomer tube within the bubble column. Another liquid rate estimation method was developed using the calculated liquid hold-up measurement in the riser section and actual volumetric gas rate exiting the column. This method assumes that all liquid entering the riser from the bubble column is entrained with the gas (i.e., no liquid recirculation was assumed to occur within the riser section). In this case, the liquid recirculation rate was estimated to be between 2-6 LPM (in terms of turnover rate, 1.5-0.5 min^{-1}, respectively) and was dependent on superficial velocity and independent of column pressure.

Future cold model tests will focus on effects of different liquid and solid media on the flow dynamics within the column. In these tests, the problems associated with catalyst settling and dispersion will be studied. Other options for directly measuring the liquid recirculation rate will also be investigated.

NOMENCLATURE

A_c Cross sectional area of the diptupe, m^2

$D_{diptube}$ Internal diameter of the diptube, m

h_1 Length of lower column differential pressure measurement, m

h_2 Length of upper column differential pressure measurement, m

h_3 Length of riser differential pressure measurement, m

h_{column} Total height of liquid head in the bubble column, m

$h_{diptube}$ Height of liquid head in the downcomer/diptube, m

h_r Height of liquid head in the riser tube section, m

h_{ref} Reference height elevation (bottom of the bubble coulmn), m

P_A Reactor at liquid surface in the overhead separation vessel, N/M^2

P_B Reactor at exit of the diptube near the bottom of the bubble column, N/M^2

P_{rxtr} Reactor pressure, PSI

Q_G Volumetric rate of gas exiting the reactor, $m^3\ s^{-1}$

Q_L Volumetric rate of liquid recirculating through the diptube, LPM or $m^3\ s^{-1}$

SV   Gas space velocity, SL h^{-1} Fe·g^{-1}

TOS   Time-on-stream, hours

u_A Liquid velocity at liquid surface in the overhead separation vessel, $m\ s^{-1}$

u_B Liquid velocity at the exit of the diptube, $m\ s^{-1}$

U_g Superficial gas velocity based on inlet reactor conditions, $cm\ s^{-1}$

U_L Superficial liquid velocity, $cm\ s^{-1}$

w.c.   Pressure in units of water column, inches

e_g Gas hold up fraction, $L\ L^{-1}$

e_{gc} Gas hold up fraction in the bubble column, $L\ L^{-1}$

e_{gr} Gas hold up fraction in the riser tube, L L^{-1}

e_L Liquid hold up fraction in the reactor vessel, L L^{-1}

e_s Solid volume fraction, L L^{-1}

r_s Density of the liquid (slurry) in the bubble column, kg/m^3

REFERENCES

1.   B. H. Davis, "Technology Development for Iron and Cobalt Fischer-Tropsch Catalysts," Quarterly Report #3, DE-FC26-98FT40308, April - June, 1999.

2.   B. H. Davis, "Technology Development for Iron and Cobalt Fischer-Tropsch Catalysts," Quarterly Report #3, DE-FC26-98FT40308, July - August, 1999.

3.   B. H. Davis, "Technology Development for Iron and Cobalt Fischer-Tropsch Catalysts," Quarterly Report #3, DE-FC26-98FT40308, October - December, 1998.

4.   B. H. Davis, "Technology Development for Iron and Cobalt Fischer-Tropsch Catalysts," Quarterly Report #3, DE-FC26-98FT40308, January - March, 1999.

5.   Fan, Liang-Shih, *Gas-Liquid-Solid Fluidization Engineering*, Butterworths Series in Chemical Engineering, 1989, ISBN 0-409-95179-X..

6.   O'Dowd, W., J. Ruether, and S. Saxena, *AIChE J.*, Vol.33, No. 12, pg. 1959-1970, December 1987.

7.   Saxena, S.C., M. Rosen, D.N. Smith, and J.A. Ruether, Chem. Eng. Commun., Vol 40 pp. 97-157.

8.   Krishna, R., Oil & Gas Science and Technology, Vol. 55 (2000), No. 4, pp. 359-393.

9.   Krishna, R., J.M. van Baten, M.I. Ureanu, and J. Ellenberger, Catalysis Today, 66 (2001), 199-207.
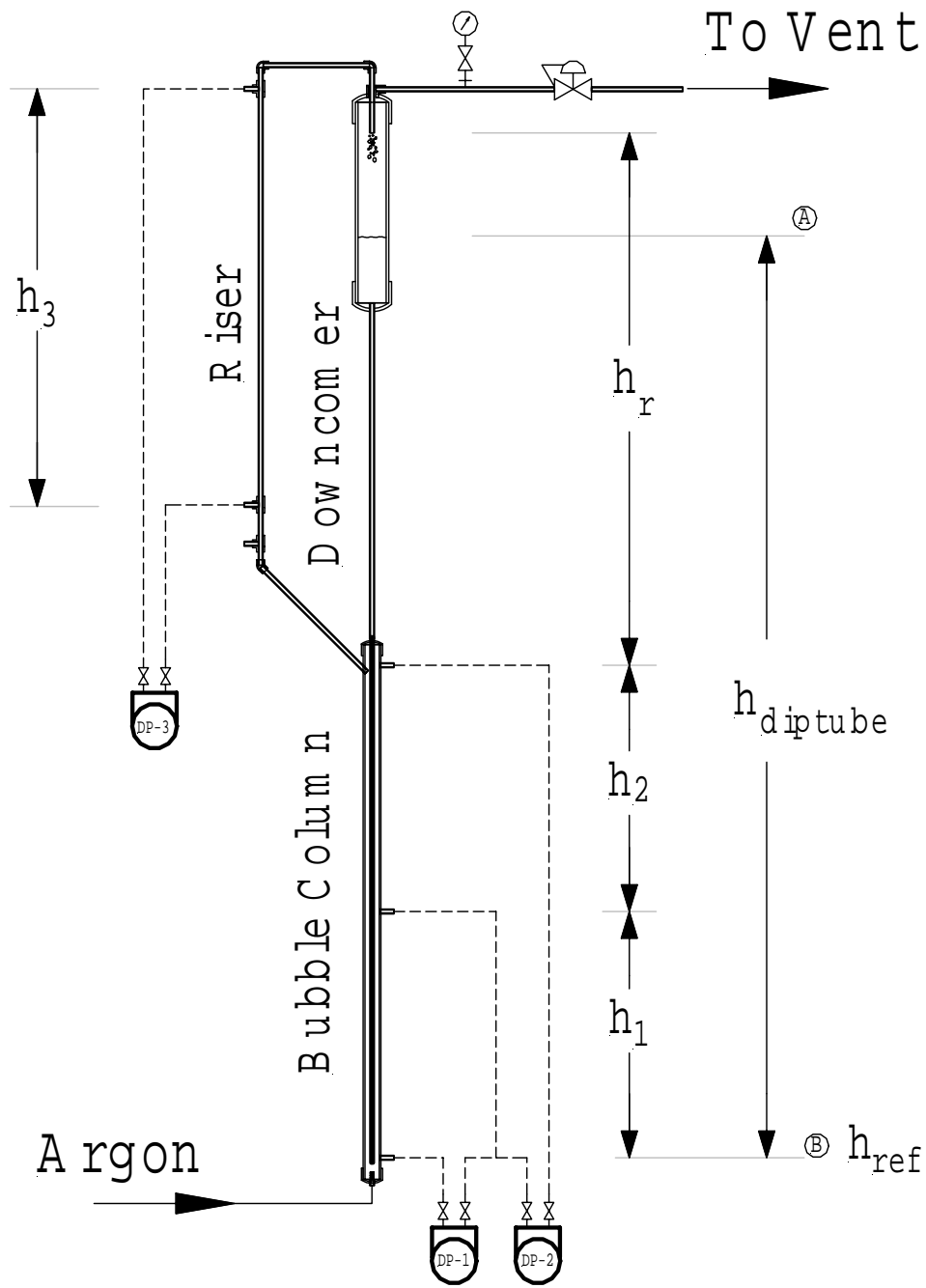
Figure 1.   Schematic of the CAER SBCR Cold Model.
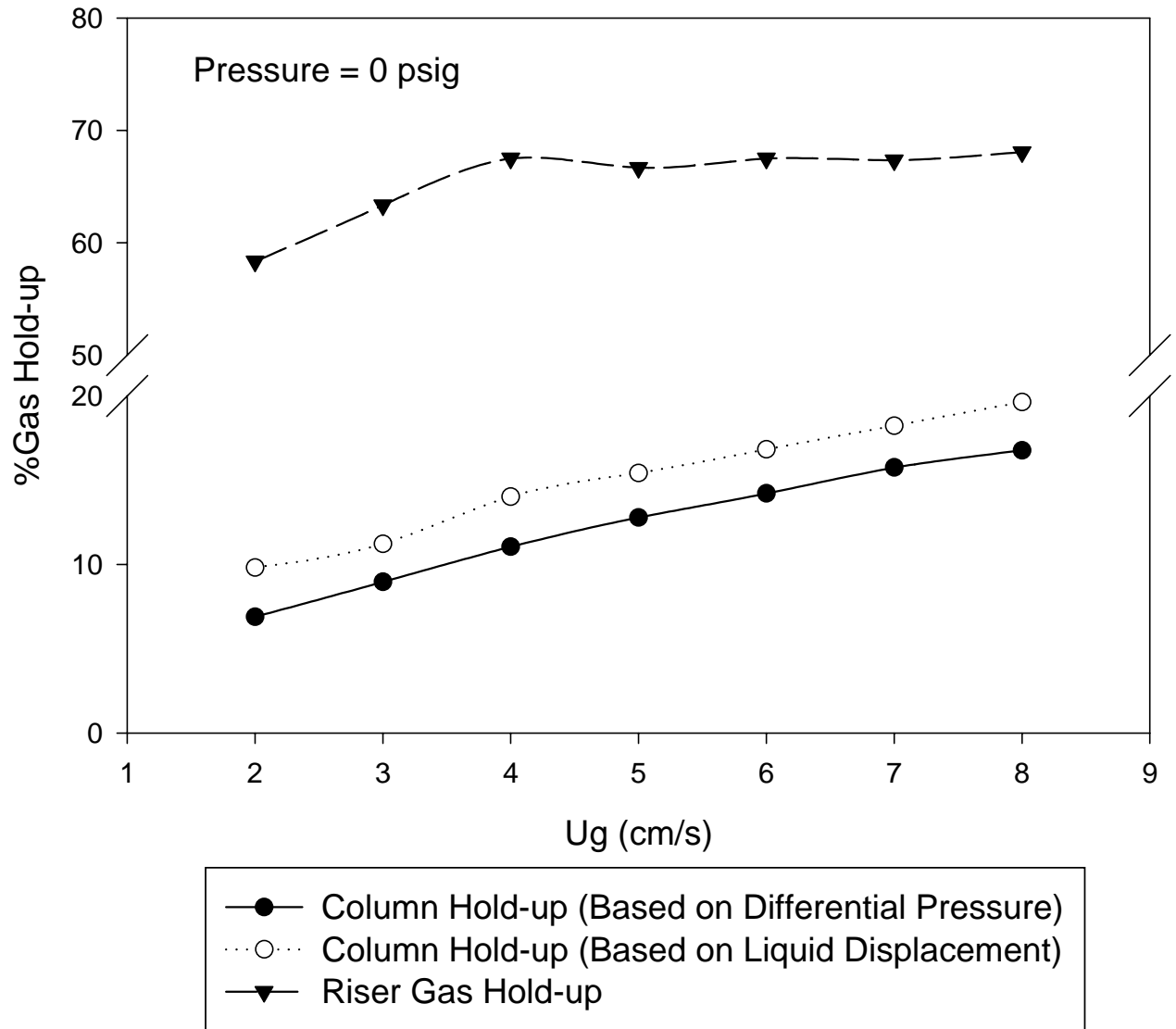
Figure 2.   Effect of inlet gas superficial velocity of gas holdup (0 psig, water Argon system).
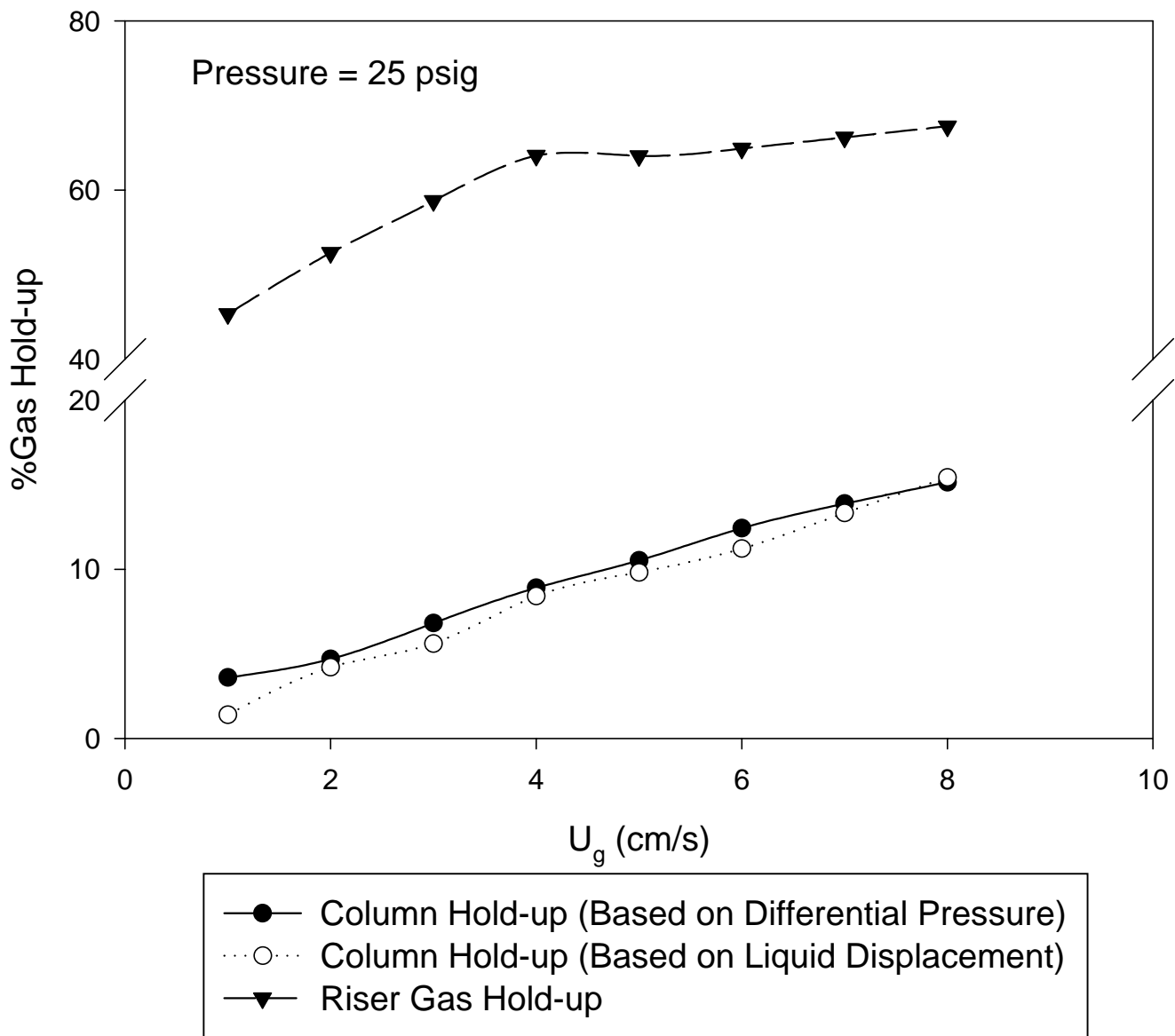
Figure 3. Effect of superficial velocity on gas holdup (25 psig, water/argon).
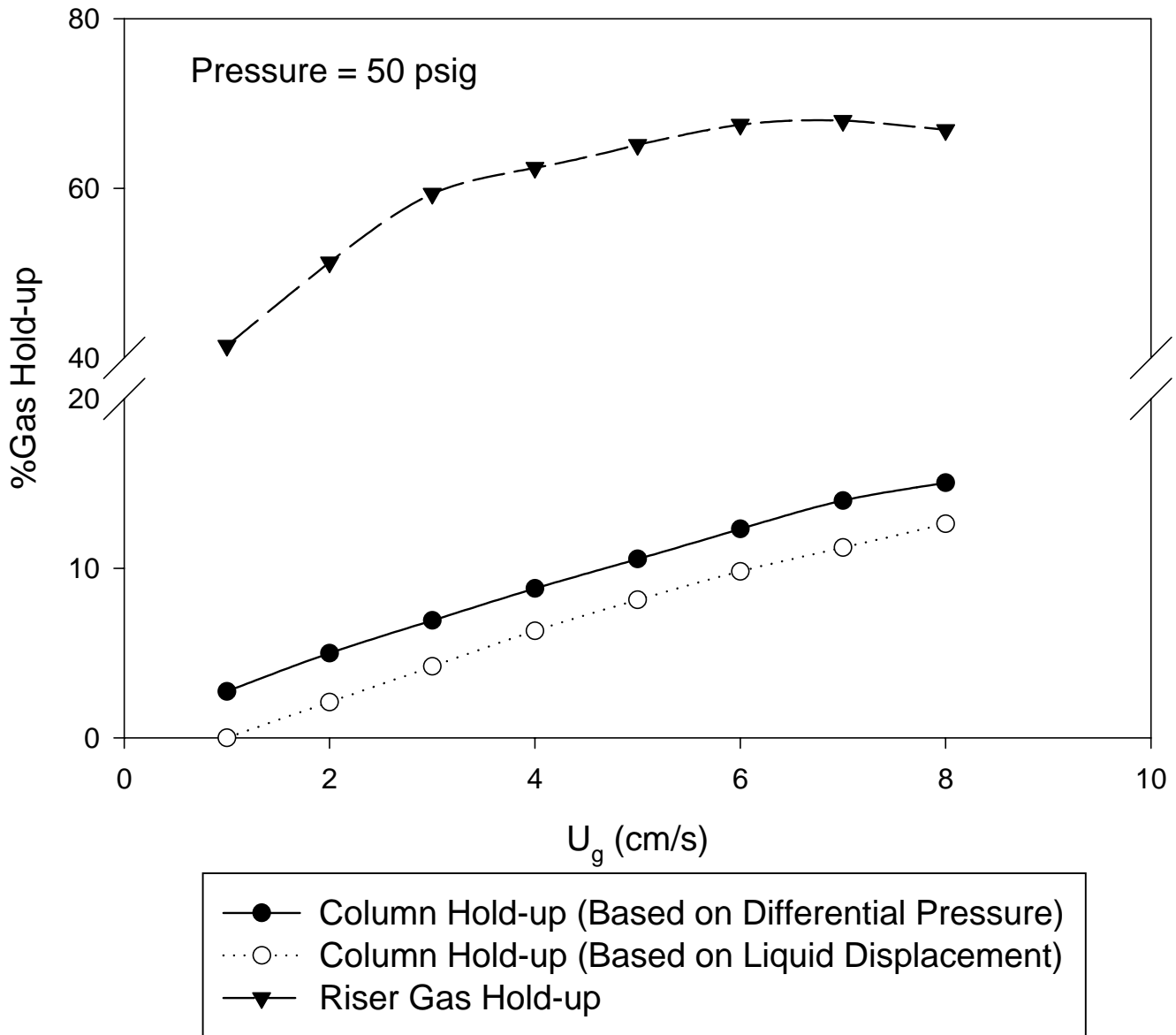
Figure 4.   Effect of superficial velocity on gas holdup (50 psig, water/argon).
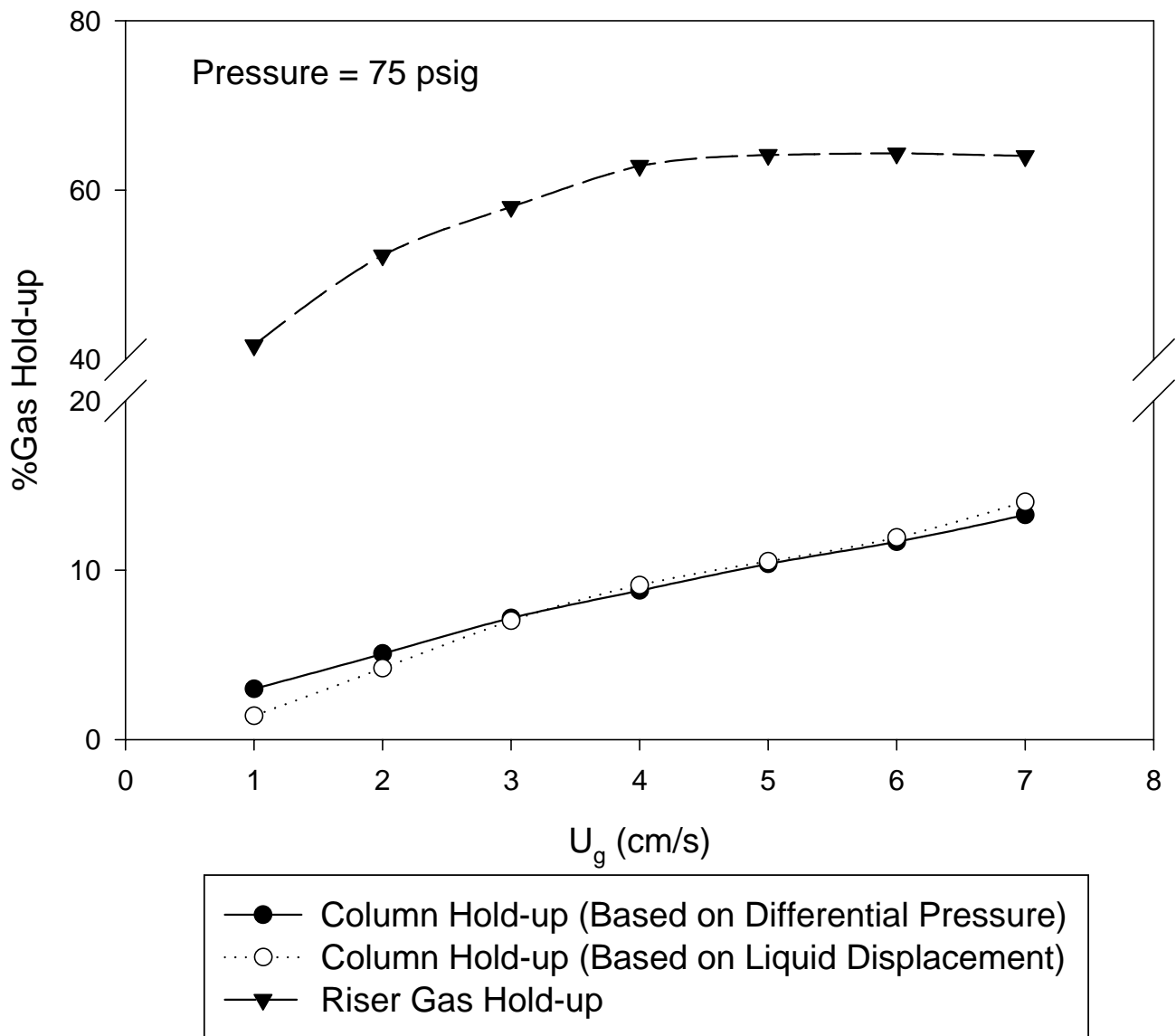
Figure 5.   Effect of superficial velocity on gas holdup (75 psig, water/argon).
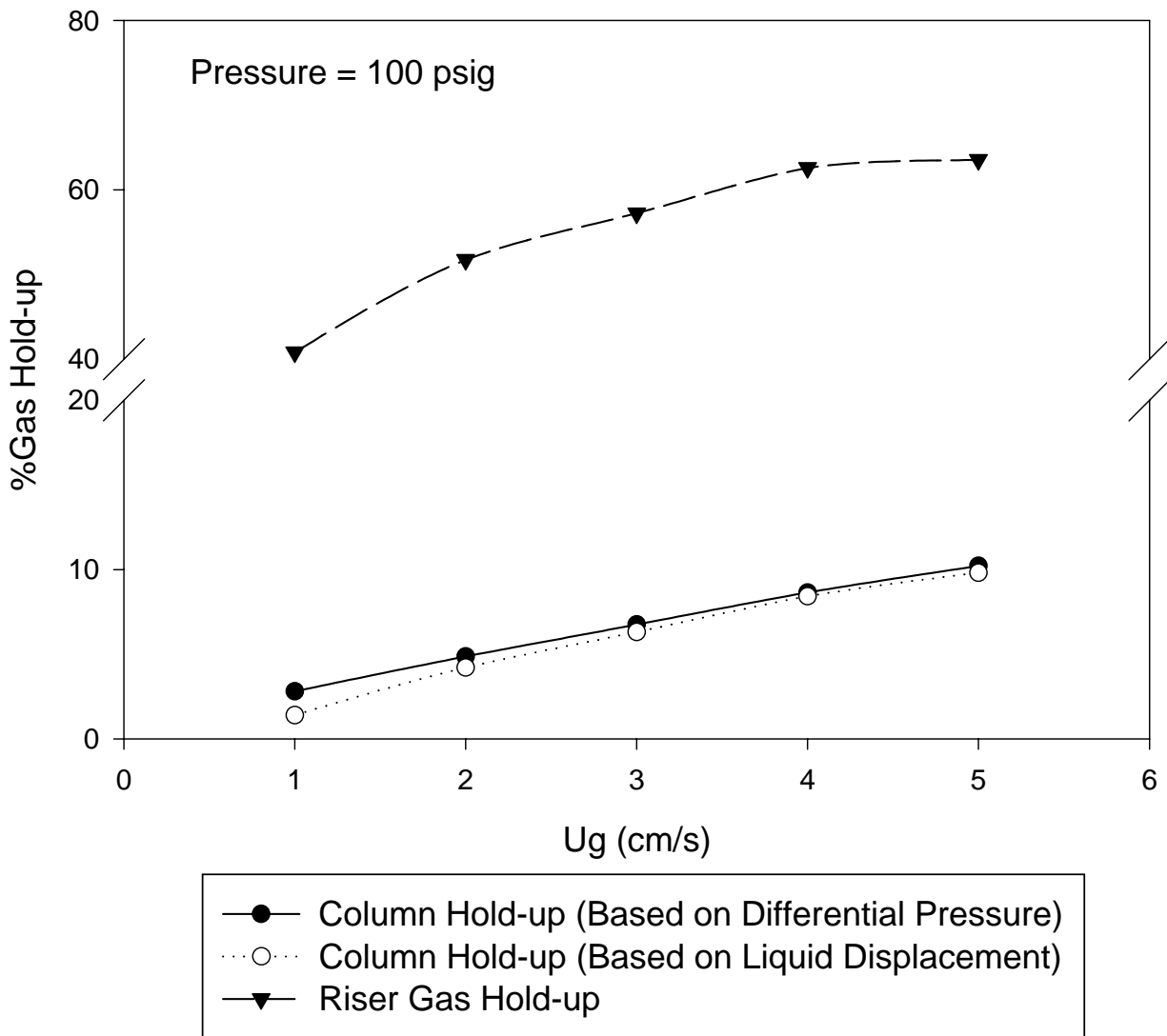
Figure 6.   Effect of superficial velocity on gas holdup (100 psig, water/argon).
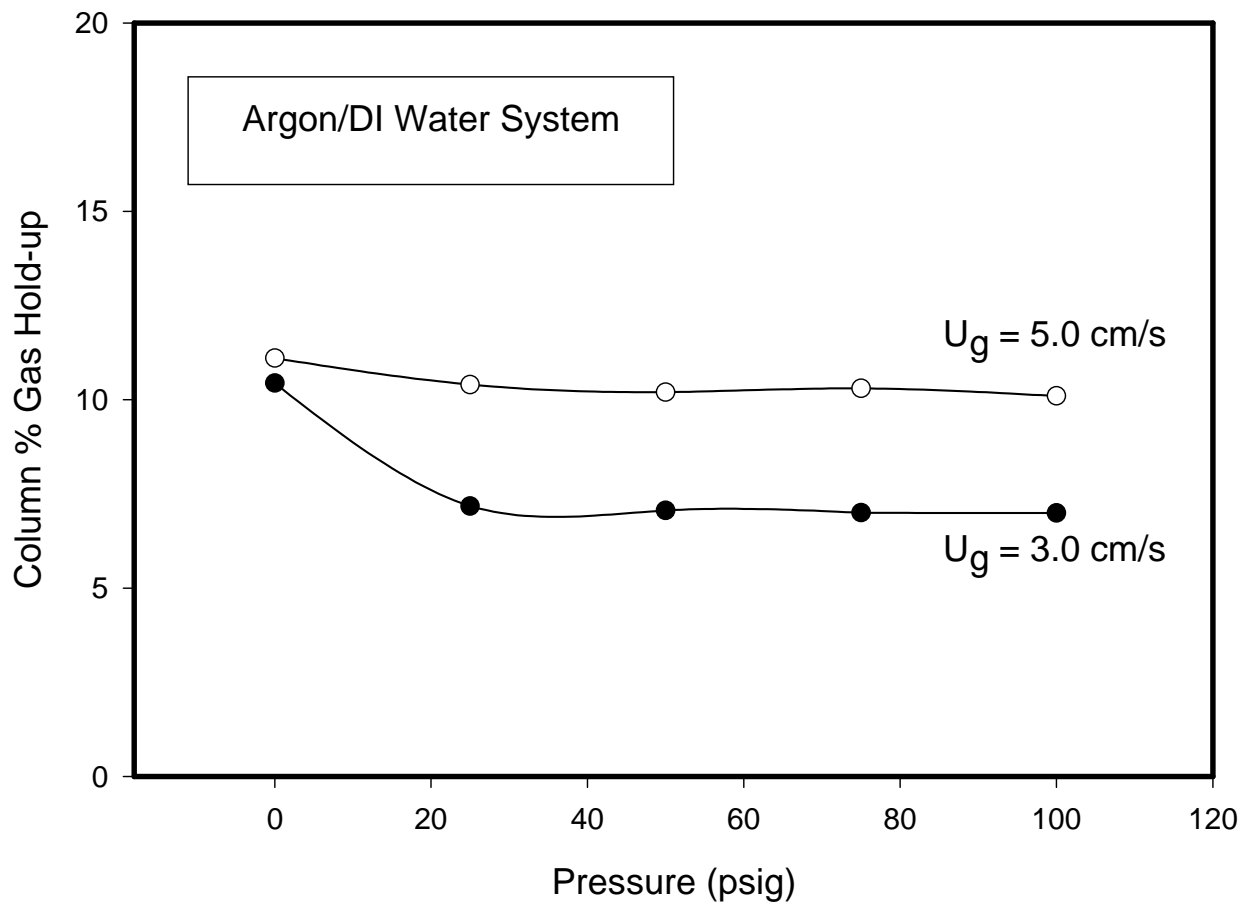
Figure 7.   Effect of pressure on column gas holdup.
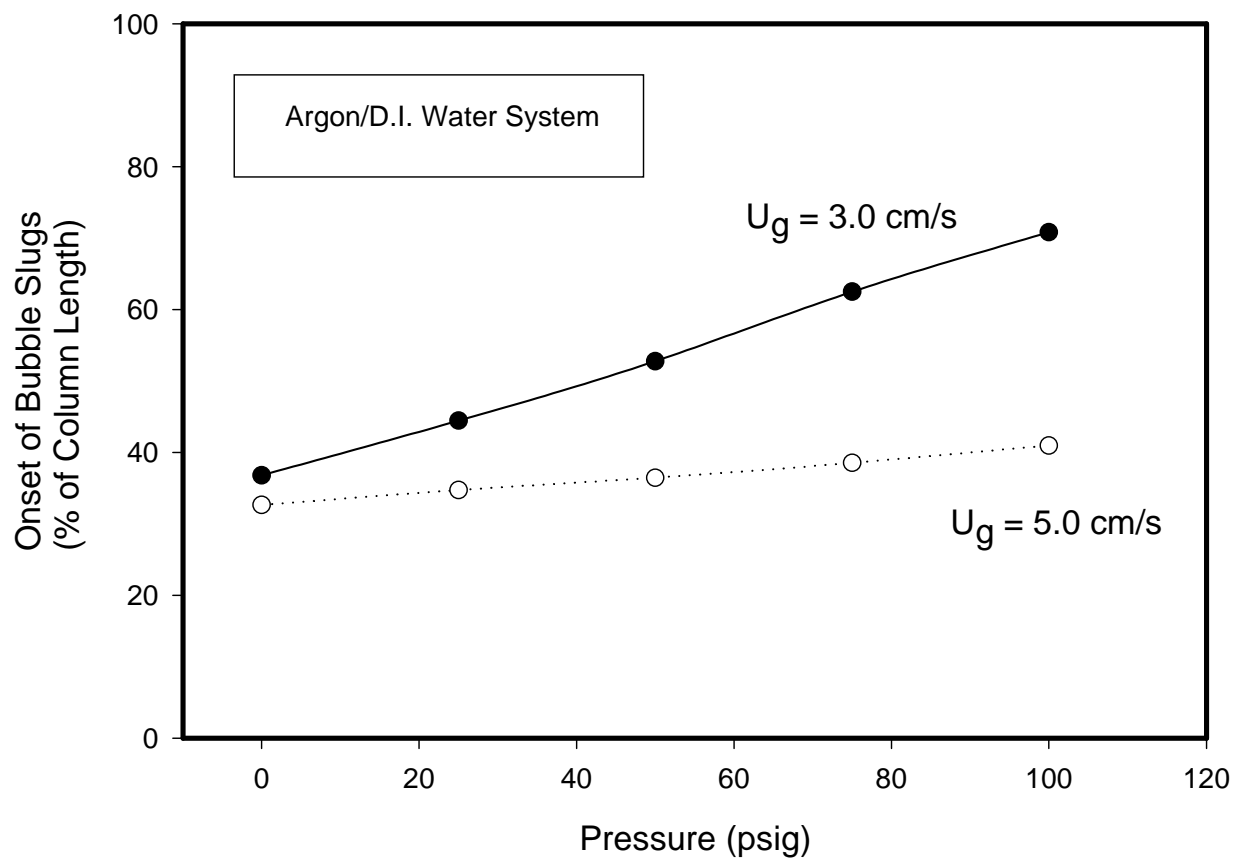
Figure 8.   Effect of column pressure on bubble slugging onset.
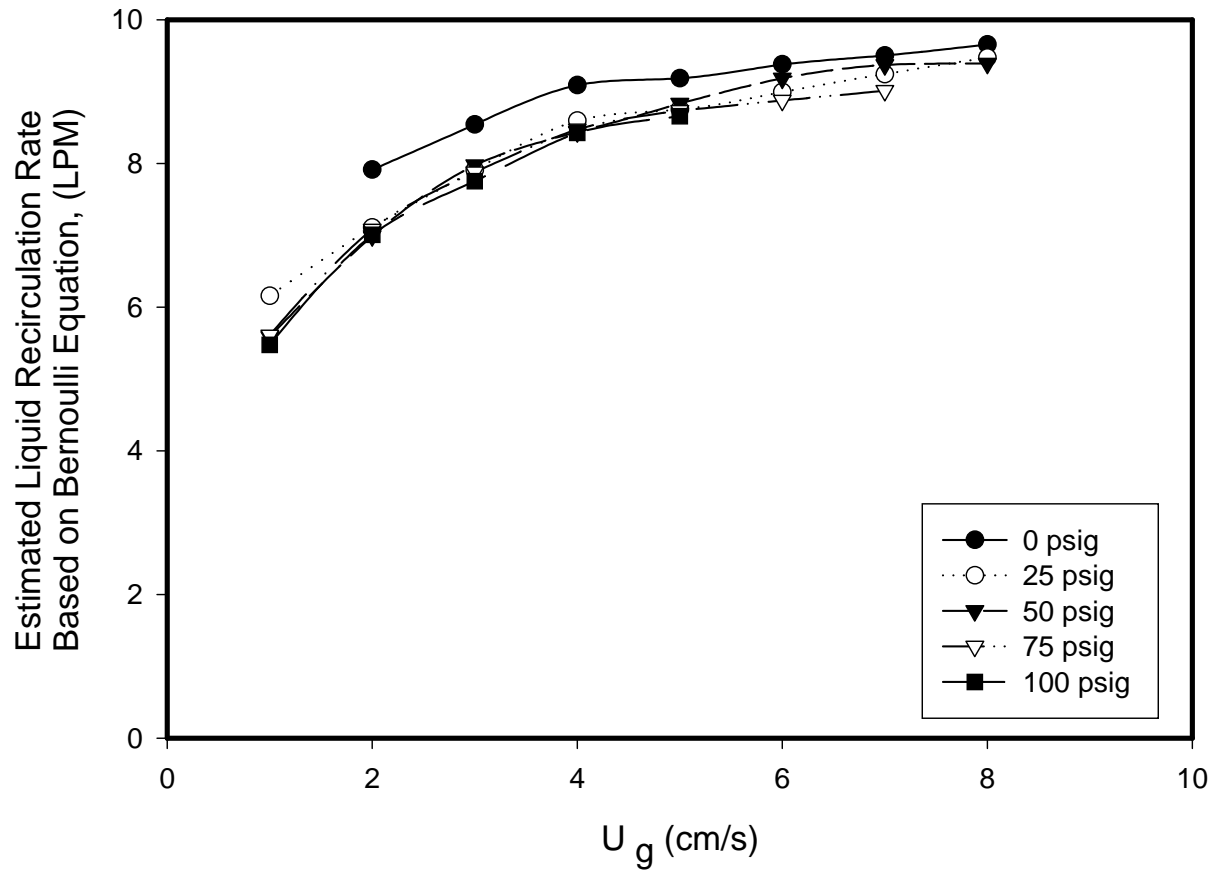
Figure 9.   Maximum estimated liquid recirculation rate based on the Bernouli Equation
                (Mechanical Energy Balance).
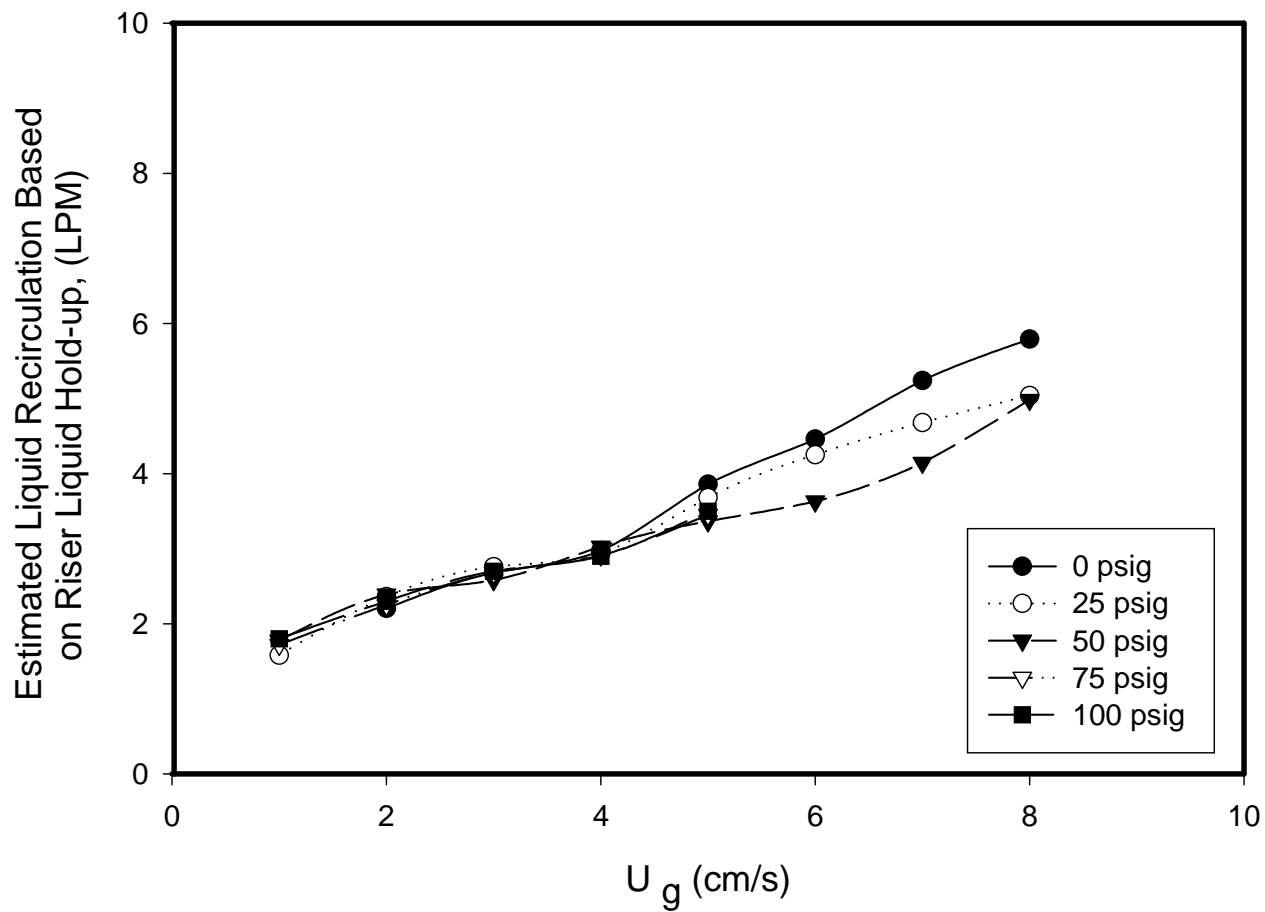
Figure 10.   Estimated liquid recirculation rate based on the riser gas Hohdup and gas
volumetric rate.
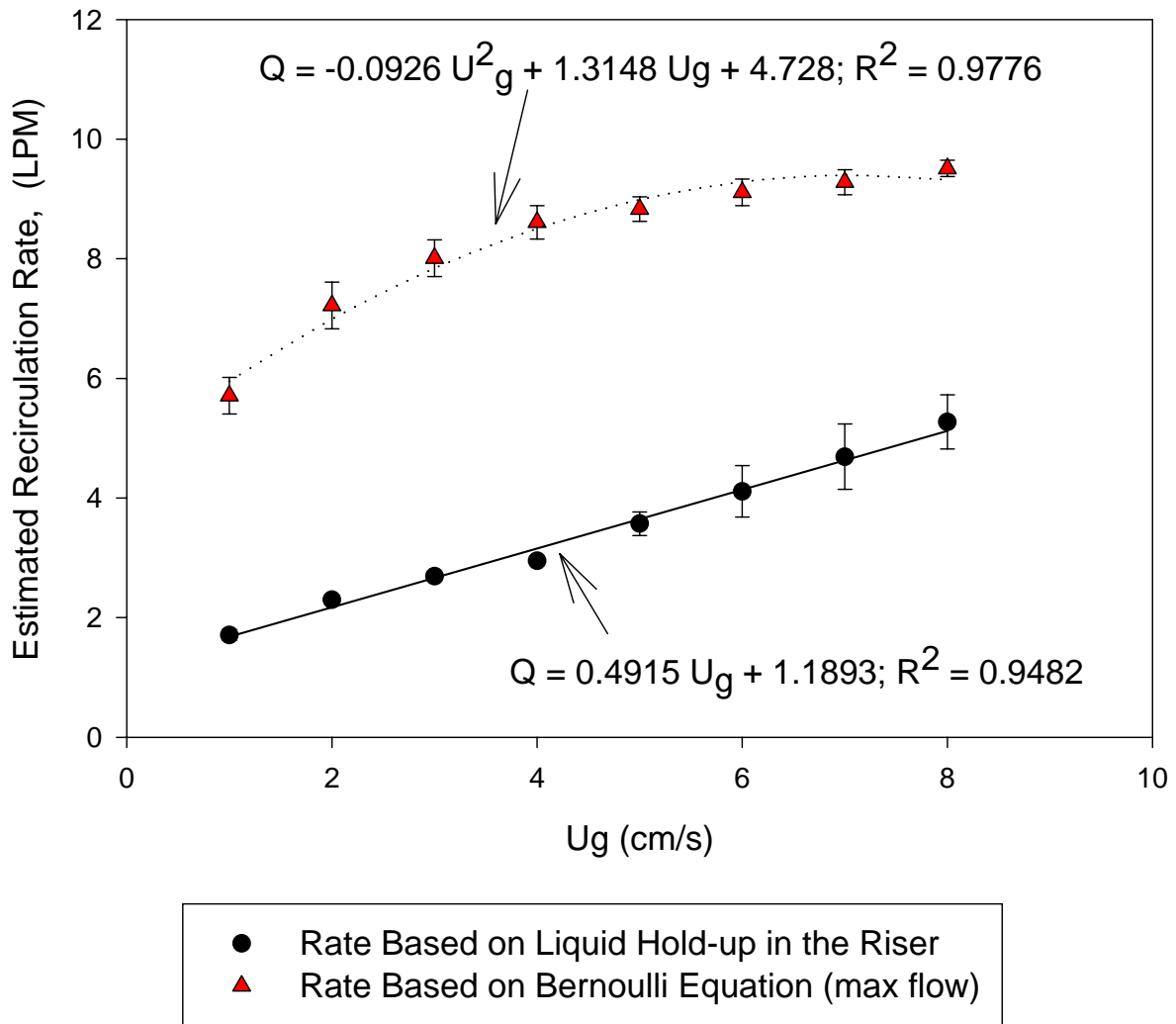
Figure 11.   Comparison of liquid recirculation method estimation results.

Task 5. Oxygenates

The objective of this task is to obtain a better understanding of the factors that affects catalyst selectivity toward oxygenates for iron-based Fischer-Tropsch catalysts.

No scheduled activity to report.

Task 6. Literature Review of Prior Fischer-Tropsch Synthesis with Co Catalysts

The objective of this task is to prepare a critical review of prior work on cobalt Fischer-Tropsch catalysts.

No scheduled activity to report.

Task 7. Co Catalyst Preparation

The objective of this task is to prepare a limited number of cobalt-based Fischer-Tropsch catalysts that can be used to obtain baseline data on cobalt-based Fischer-Tropsch synthesis.

No scheduled activity to report.

Task 8. Cobalt Catalyst Testing for Activity and Kinetic Rate Correlations

The objective of this task is to conduct initial screening of the cobalt catalysts prepared in Task 7 to select three baseline catalysts that will then be used to generate a data base on the performance of cobalt-based Fischer-Tropsch catalysts in slurry reactors.

No scheduled or further activity to report.

Task 9. Cobalt Catalyst Life Testing

The objective of this task is to obtain life data on baseline cobalt Fischer-Tropsch catalysts.

No scheduled for further activity to report.

Task 10. Cobalt Catalyst Mechanism Study

The objective of this task is to determine the impact of secondary reactions on the relationship of cobalt Fischer-Tropsch catalysts under conditions appropriate to slurry bubble column reactors.

Task 11. University of California, Berkeley (Subcontract)

The objective of this task is the characterization of the structure and function of active sites involved in the synthesis of high molecular weight hydrocarbons from CO and H_2 on multi-component catalysts based on Fe as the active component.

Table Of Contents

I.   FISCHER-TROPSCH SYNTHESIS ON IRON CATALYSTS

1.   Calculation of the amount of adsorbed CO on catalyst surface at FTS reactions

1. Material balances

In order to determine the amount adsorbed on the surface two kinds of response curves have to be measured. In the first case the adsorption should be disclosed. This could be done by either by applying a non-adsorbable tracer gas, or by replacing the catalyst with an inert solid. The latter approximation was tested first. The micro-fluid reactor was filled with graphite with the same volume as that of the catalyst. The experiments were carried out in a micro–fluid reactor at 523K and 0.1 MPa, with $H_2/CO/Ar$ ratio of 5/1/6 and with a total flow rate of 60 ml/min. The response curve of a switch between ^{12}CO and ^{13}CO was obtained.

In a separate experiment the reactor was filled with 0.3 g $Fe-Zn-K_8-Cu_4$ catalyst (60-80 mesh). The same response curves were recorded at the same conditions. The conversion was 8.0 %. In the FT reaction the CO adsorption is reversible and the surface reaction of the adsorbed CO is irreversible. In this case there is a compartment model of CO that is an isolated part of the total reaction mechanism. This compartmental model is plotted in Fig. 1.

Figure 1.
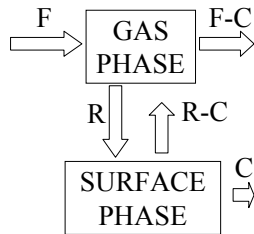
where
F is the total CO feed rate,
C is the conversion rate
R is the adsorption rate, all in mol/sec dimension and at steady state.

Let us consider a steady-state transient labeled experiment with ^{13}CO down step forcing function.
The material balances in the micro-fluid reactor can be calculated directly based on the response curves. The corresponding curves are plotted in Fig.2. In order to keep the figure simple an ideal step-like forcing was assumed.

Figure 2.
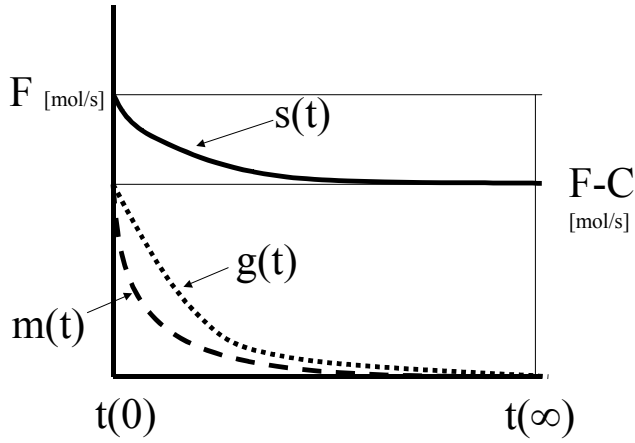
The material balance of the labeled material from time=0 to the end of the experiment can be described as follows:

$$Q_T = Q_G + Q_S = \int_0^\infty (F - C) g_{CO}(t) dt + \int_0^\infty C s_{CO}(t) dt \qquad (1)$$

where
$g_{CO}(t)$ is the gas phase response of CO
$s_{CO}(t)$ is the surface response of CO
Q_T is the total CO capacity
Q_G is the gas phase CO capacity
Q_S is the surface phase capacity

The left side of Eq. 1 is the total labeled CO that was in the system at the start of the experiment. The first term on the right side is the amount that left the system in form of CO through the gas phase. The second term is the amount of CO that reacted and left the system via surface reaction. The gas phase capacity can be expressed by m(t) curve according to Eq. 2:

$$Q_G = \int_0^\infty (F - C)(m(t) dt \qquad (2)$$

where:
m(t) is the measured mixing curve, i.e. the "non-adsorbing" response.

Based on Eq. 1. and 2. Q_S the surface capacity of CO can be calculated as

$$Q_S = Q_T - Q_G = \int_0^\infty (F - C)g_{CO}(t)dt + \int_0^\infty Cs_{CO}(t)dt - \int_0^\infty (F - C)m(t)dt$$

It has to be noted that two areas, under g(t) and under s(t) as well have to considered in order to get the total amount of adsorbed CO.

In general case this is a single parameter model. The Q_S and s(t) can be obtained by estimating R, the adsorption rate.

If R is fast enough then g(t) = s(t) . In this case there is no need for R to calculate Q_S. Nevertheless, the integration has to be done in the same way, i.e. both of the areas have to be considered.

Here has to be noted that the graphite has different pore structure compared to the Fe-Zn based catalyst. This can affect the measured surface capacity. The extent of this can be estimated by completing the experiment with non-adsorbable tracer gas.

The measured m(t) and g(t) curve is plotted in Fig. 3.

Figure 3.
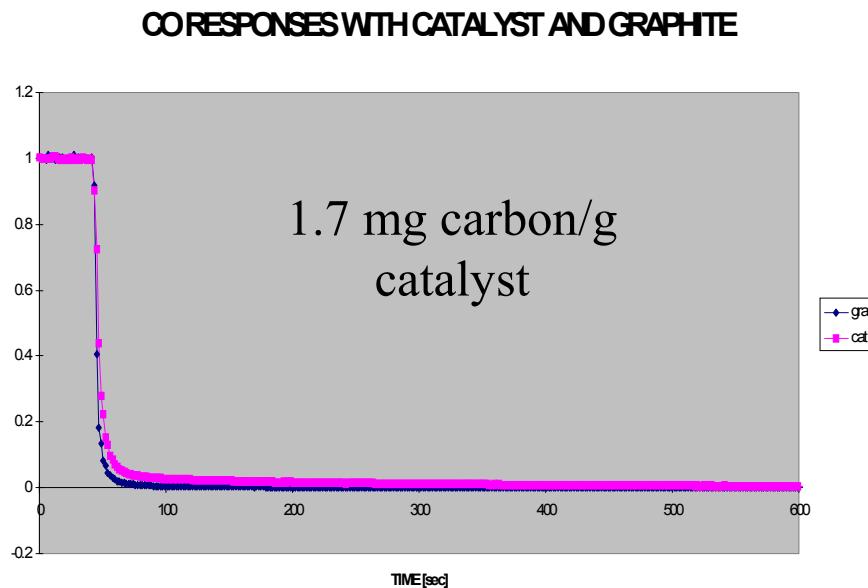
The steady state surface CO capacity is 12.7 mmol/g. at. Fe.

2. Response curves of product materials

In the FT reaction there are several products forming on the surface simultaneously. The response curves of products can be monitored following the signal of the mass spectrometer at different masses. The derivative of the up-step responses provides information of the residence times of product materials. Some selected curves of this kind are presented in Fig. 4.

IMPULSE RESPONSES OF DIFFERENT COMPOUNDS DERIVED FROM STEP RESPONSES
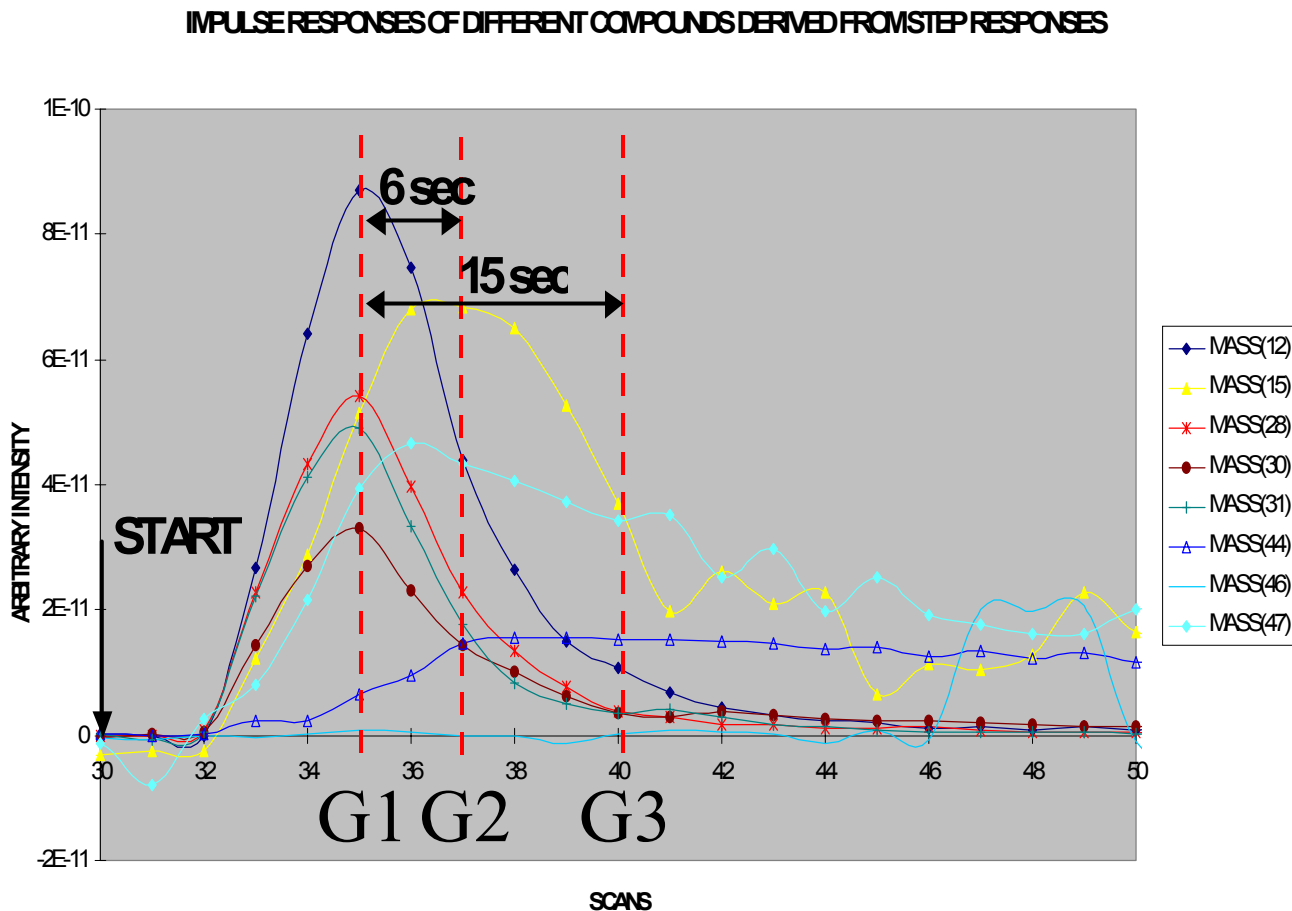
There are three main groups that can be distinguished based on this figure. Group 1 (G1) contains the starting CO and some methanol and ethanol fragments. Group 2 (G2) contains the methane related Mass(15) peak and probably more paraffin related fragments. The broad line marked with triangles represents the CO_2 response with maximum at G(3).

Further experiments are in progress in order to improve the fragment identification and time resolution.

II. FISCHER-TROPSCH SYNTHESIS ON COBALT CATALYSTS

1. The Effect of Water on the Fischer-Tropsch Synthesis: Reaction Rates, Selectivity, and Active Carbon Coverage on Cobalt Catalysts

Introduction

The Fischer-Tropsch Synthesis (FTS) is the catalytic conversion of carbon monoxide and hydrogen into a complex mixture of paraffins, olefins and oxygenates. Co-based catalysts, employed extensively for FTS, are characterized by their high activity and predominantly paraffinic product distribution. H_2O is the main oxygenated product and its presence in high concentrations in typical FTS reactors makes it essential to determine the effect of water on the FTS rates, product selectivities and the chemical nature of the active sites. Some studies have shown that Co catalysts supported on Al_2O_3 (1-3) and catalyst with small crystallites (4), tend to deactivate in the presence of water due to oxidation and sintering of the active metallic Co crystallites. Kim (5), Iglesia (6) and Schulz *et al*. (7), however, reported an increase of the rate of CO consumption on Co/SiO_2, Co/TiO_2 and $Co-Mg-Th-SiO_2$ catalysts when the partial pressure of water is increased either by raising the CO conversion or by co-feeding water with the reactants. They also observed that water tends to increase the molecular weight of the products, by increasing the C_{5+} selectivity and decreasing the CH_4 selectivity. Still the reasons for the benign effects of water on rate and selectivities on silica- and titania-supported cobalt catalysts are unclear. One possible explanation is that water directly takes part in the mechanism for the consumption of CO, through a path parallel to the classic mechanism described by the carbide theory (8-10). An enhancement of the reaction rate, though, is consistent with a higher coverage of the surface by hydrogen (8-10), whereas a lower methane selectivity would arise from a smaller amount of hydrogen on the catalyst (8-10): these features lead to the conclusion that water can not be a hydrogen donor. Therefore, in this mechanistic view, H_2O would react directly with some form of adsorbed carbon and hence contribute to the formation of a chain growth monomer. Our recent studies however, showed that the kinetic isotope effect (k_H/k_D) for the overall CO consumption on a Co/SiO_2 catalyst is independent of the CO conversion and hence of water partial pressure (11). Given these premises, the presence of a parallel way of consuming CO through the addition of water seems to be very unlikely. On the other hand, Iglesia (5) proposed that a separate intrapellet water phase could form, enhancing the diffusion of the reactants through the catalyst pores and thus increasing the accessibility of isolated transport-limited regions within porous pellets. An alternate unexplored explanation for the water autocatalytic effect on Co/TiO_2 and Co/SiO_2 catalysts during FTS is that the presence of H_2O affects the number of active sites, by inhibiting either the site deactivation or the formation of less reactive carbon. In a parallel study, we have utilized *in situ* FTIR spectroscopy to monitor the density of CO-binding sites with changes in water concentration during FTS (12). It was found that the coverage by CO does not increase in the presence of water. In this paper, we test whether water influences the concentration of carbonaceous species on the catalyst under reaction conditions.

Various researchers have presented techniques to estimate the amount of reactive carbon present on the catalytic surface. Winslow and Bell (13) determined the carbon coverage on a Ru/TiO_2 catalyst at 463 K and 0.08 MPa by titration with D_2, by following the evolution of CD_4 (attributed to the hydrogenation of chemisorbed carbon) with time. Two CD_4 peaks were

detected, the first one being representative of reactive carbon (named by the authors as Carbon α). The authors, following Bianchi *et al.* (14) and Bianchi *et al.* (15), who performed similar studies on an iron catalyst at atmospheric pressure, stated that the second peak is due to hydrogenation of a pool of less reactive carbon (carbon β). In a different approach, Winslow and Bell (16) estimated the amount of carbon α from the decay with time of the flow rate of ^{13}CO after the feed of the reactor was changed from a $^{13}CO/H_2$ mixture to a $^{12}CO/H_2$ mixture; CD_4 that was observed upon feeding D_2 to the reactor after the first transient was completed, was attributed to hydrogenation of carbon β. A similar isotope exchange approach was also adopted by De Pontes *et al.* (17) on Ru/TiO_2 and Ru/SiO_2 to detect the presence of two pools of adsorbed carbon. Despite the fact that Co is one of the most important and widely used catalyst for FTS, very few studies have been carried out at high-pressure reaction conditions to estimate the number of active carbon atoms during FTS on these catalysts. Biloen *et al.* (18) presented data collected on an unsupported Co catalyst at 488 K, 0.3 MPa and a H_2/CO ratio of ~5:1, with $^{12}CO/H_2$-$^{13}CO/H_2$ switch experiments, similar to the ones previously described. Finally, Mims and McCavendish (19) have also performed carbon coverage with an identical approach on a Co/SiO_2 catalyst.

In this work the effect of water on rate, selectivities and carbon coverage on supported cobalt catalysts at FTS reaction conditions is presented. We have attempted to determine if the observed rate enhancements by water would correspond to an increase in the active carbon coverage on Co catalysts.

Experimental Approach

Catalyst synthesis and characterization

The 21.9% Co/SiO_2 and 15% Co/TiO_2 catalysts were prepared by impregnation of standard solutions of $CoNO_3 \cdot 5H_2O$ onto SiO_2 (Grace-Davison) and TiO_2 (Degussa) respectively. The impregnated samples were dried in air at 333 K for 24 h. They were subsequently reduced in flowing hydrogen (24 x 10^3 cm^3/h, 0.167 K/s from 313 K to 423K, 0.0083 K/s from 313 K to 623 K, hold for 1 h for the SiO_2-supported sample; and 15 x 10^3 cm^3/h, 0.0167 K/s from 313 K to 673K, hold for 16 h for the TiO_2-supported sample). The catalysts were then passivated with 1% O_2 in He for 1 h at ambient temperature. The Co metal dispersion of the Co/SiO_2 batch was measured by chemisorption uptake experiments at 373 K (Autosorb-1, Quantachrome) and was found to be 4.6% assuming a 1:1 H:Co soichiometry (19, 20).

Measurement of steady state and transient FTS kinetics

Steady state and transient kinetic data were collected using a SS304 fixed-bed reactor (0.95 cm outer diameter and 0.5 cm inner diameter) placed in a three-zone furnace (Electro Power Controls, Inc.), with the catalyst bed temperature profile being monitored precisely with a movable K-type thermocouple. Synthesis gas (CO 31%, H_2, 62%, and Ar 7% used as internal standard, 99.99% purity, Praxair), was first purified using an activated charcoal trap (Sorb-Tech RL-13) to remove carbonyls and a molecular sieve trap (Matheson, Model 452 A) to remove water. Hydrogen (99.999%, Bay Airgas) was also purified using a molecular sieve trap (Matheson, Model 452 A) and an oxygen trap (Matheson, Model 64-1008A). These gases were

metered using mass flow controllers (Brooks, Model 5850-CAB1AF1A3) and the flow of synthesis gas or H_2 was directed either to the reactor or to the vent with a 4-port valve, mounted close to the reactor inlet. A 1/16" capillary tube was positioned under the bed and was utilized to divert a part of the effluent stream (~10 %) into a differentially pumped atmospheric sampling system connected to a quadrupole mass spectrometer (Leybold Inficon Instruments Co., Inc.), allowing to continuously collect gas samples during the runs. This step minimized the total dead volume between the reactor and the mass spectrometer. In addition, two needle valves were utilized in order to maintain the desired pressure drop between the reactor zone (at high pressure) and the tube to the mass spectrometer (under vacuum). The heavier products (waxes) leaving the reactor were collected in a bottle kept at 393 K and high pressure, whereas the remaining products were sent through a back pressure regulator (Mitey Mite) to a gas chromatograph (HP 5890 Series II) equipped with a porapak Q packed column (15.2 cm × 0.318 cm) and a cross-linked methyl silicone capillary column (HP-1, 50 m × 0.32 mm; 1.05 μ film), connected to a Thermal Conductivity Detector and a Flame Ionization Detector respectively. This enabled the analysis of all hydrocarbons (C_1 to C_{12}), H_2, Ar, CO, CO_2 and H_2O. The organic and aqueous phases were collected in another bottle after the GC at ambient conditions. All the lines were heat-traced to >393 K, to avoid condensation of the heavier hydrocarbons.

Active carbon coverage measurements were conducted at steady state FTS conditions, by performing rapid switches of the feed to the reactor from synthesis gas to H_2 at high pressure, followed by monitoring of the transients of different components with the mass spectrometer. The details related to calculation of the active carbon coverage are presented in the Results and Discussion section separately.

Results and Discussion

Steady state FTS activity and selectivity measurements

Kinetic runs were conducted on two batches of catalysts. No significant enhancement of the rate of consumption of CO was observed on the silica-supported catalyst with the increase of the concentration of the indigenously present water, from 0.002MPa to 0.010 MPa, at 0.5 MPa and 453 K, as evident from Figure 1. On the other hand, an increase in the water concentration, led to a decrease in the methane selectivity and an increase in the C_{5+} selectivity (Figure 2). The effect of the partial pressure of internally generated water on olefin selectivity is affected by the parallel effect of contact time. The combined result is reported in Figure 3 as the ratio of pentane to pentane: the observed decrease in olefin content with partial pressure of water produced is to be attributed to extensive readsorption of α-olefins into the growing chain mechanism at higher contact times (10).

The experiments performed on the Co/TiO_2 catalyst at 2 MPa and 473 K showed a significant correlation between water partial pressure, methane and olefin selectivity and also rate of CO consumption. In particular to an increase of the water partial pressure, either by increasing the CO conversion or by introducing it from outside, corresponded a significant increase of the rate of consumption of CO (Figure 4), and of C_{5+} selectivity (Figure 5) together with a decrease of methane selectivity (Figure 5).

Several studies have attempted to shed light on the possible roles of H_2O on selectivity and rates during FTS reactions. Schulz *et al.* (6) proposed that Co surfaces contain distinct methanation and chain growth sites and that H_2O titrated the former type of sites leading to a

decrease in the CH_4 selectivity. Water has been shown to inhibit olefin hydrogenation (23) and the termination of chains by H* addition during FTS (5). The marked effect of water in the inhibition of chain termination to paraffins remains unexplained; it appears to reflect lower concentrations of adsorbed hydrogen during FTS. Adsorbed hydrogen is required for the formation of the CH_x monomers involved in chain growth and thus the concurrent increase in FTS reaction rates would be unexpected on surfaces with less accessible adsorbed hydrogen. Iglesia *et al.* (5) proposed that an intrapellet water phase at high H_2O concentrations, can increase the rates of transport for CO, because the solubility and diffusivity of CO is higher in water than in hydrocarbon liquids (24). Intrapellet CO concentration gradients lead to lower FTS rates and C_{5+} and olefin selectivity; thus, an increase in CO diffusion rates resulting due to this intrapellet water phase could explain the changes in rates and selectivities observed at high H_2O partial pressures. The formation of this intrapellet phase will also be affected by the size of the pores, as evidenced by the lack of a significant water effect on small pore Co/SiO_2 catalysts (5). Furthermore, the addition of water catalysts did not influence reaction rates on Co-$Ru/ZrO_2/Aerosil$ (6), but led to lower rates on Co-Re/Al_2O_3 (5).

H_2O can also influence FTS rates by increasing the turnover rate or the number of exposed active sites for binding CO and hence FTS reactions. In the first possibility, H_2O may participate in CO activation pathways in addition to that with hydrogen. Recent isotopic studies, however, have failed to detect any changes in the kinetically relevant CO activation pathways when H_2O is present (11). On the other hand, the observed dependence of activity and selectivities on water partial pressures could also be as a result of different amount of carbonaceous species adsorbed on the catalytic surface, reducing the methane selectivity and enhancing the CO consumption rate on the titania-supported catalyst at high pressure. This hypothesis is here tested by means of a technique of active carbon titration with hydrogen, as described in the following section.

Estimation of Carbon coverage

When the reactor feed is changed from syngas to hydrogen, the carbon adsorbed on the surface of the catalyst during the reaction is hydrogenated mostly to methane; while at the same time, the flow rates of CO and Ar decrease to zero, and that of H_2 increases and reaches a steady value. The transients of CO, H_2 and CH_4 after a switch from syngas to hydrogen and back to syngas are presented in Figure 6. The hydrodynamics of the system is described by the following equation:

$$F(t) = F_1 + (F_2 - F_1) \cdot \left(1 - e^{-\frac{t - t_D}{\tau}} \right) \quad (1)$$

where $F(t)$ is the flow rate of an inert species as a function of the time t, F_1 is the flow rate of the same species before the switch to H_2 and F_2 is the flow rate when the transient is completed. Equation 1 results from the application of a non-stationary mass balance in the absence of reaction on a system that is combination of a plug flow reactor followed by a continuously stirred reactor. The Ar contained in the syngas mixture is the inert and internal hydrodynamic standard of the system: its flow rate transient is utilized to estimate the parameters t_D and τ in Equation 1. This model fits the decay profile of the Ar flow rate very well for all the

experimental data collected as illustrated in Figure 7. Once a reliable model for the hydrodynamics of the system is devised, the peak of methane evolved from the catalyst surface is analyzed in order to deconvolute it into two contributions; one derived from hydrogenation of a more active pool of adsorbed carbon and the other from reaction of hydrogen with a less active form of carbon on the catalyst. In order to estimate only the amount of active carbon from the methane peak, Equation 1 is applied to the decay of methane after the attainment of the maximum value in the methane flow rate profile. In fact assuming that the kinetic of formation of methane is first order with the carbon coverage and with the hydrogen coverage, and supposing that after the maximum of methane flow rate, there is no change in the concentration of adsorbed hydrogen on the catalytic surface, the decay of methane with time should follow an exponential law with a time constant τ_{CH4}. However, when the linearized flow rate $\ln[(F(t)/(F_{peak})]$ is plotted as a function of time (where $F(t)$ is the actual methane flow rate, F_{peak} the rate corresponding to the maximum of the methane flow rate), two slopes are visible, for all the experiments conducted, corresponding to two different time constants for the consumption of adsorbed carbon. An example of the presence of two distinct slopes is presented in Figure 8: from the first part of the curve a time constant of 40 s is estimated, while from the second part, the resulting value of τ_{CH4} is 315 s. The first part of the curve can be attributed to hydrogenation of active carbon, whereas the second part derives from reaction of hydrogen with some form of less reactive carbon. Since in the absence of CO, secondary reactions of FTS products are inhibited on Co catalyst at high pressure, the methane detected likely derives from hydrocracking of heavy waxes contained in the catalyst pores. Once the time constant for hydrogenation of active carbon is calculated from the first part of the methane decay, Equation 1 can be used to extrapolate the curve until the transient is completed.

$$F_\alpha(t) = F_{peak} \cdot \left(1 - e^{-\frac{t - t_D}{\tau}} \right)$$

(2)

Here, $F_\alpha(t)$ is the methane flow rate thus calculated, and $B(t)$ is the hydrodynamic decay that methane should follow in the absence of a reaction from F_{peak} to zero:

$$B(t) = F_1 \cdot \left(1 - e^{-\frac{t - t_D}{\tau}} \right)$$

(3)

The amount of active carbon adsorbed on the catalyst at the time of the switch is determined from the area between $F_\alpha(t)$ and $B(t)$ (cfr. Figure 9), after the transient is completed.

$$C^* = \int_{t_D}^{\infty} \left[F_\alpha(t) - B(t) \right] dt$$

(4)

If the Co loading and the dispersion of the catalyst are known, it is possible to calculate the percentage of the superficial Co sites occupied by active carbon.

The estimates of the carbon coverage (θ_C) of the silica-supported catalyst, at 0.5 MPa and 453 K, for which an effect on selectivity was observed, are reported in Figure 10 as a function of the water partial pressure. The values of θ_C estimated with the titration technique are

between 15% and 24% and are of the same order of magnitude of the ones reported in the literature. For example Winslow and bell (13) estimated a number of active carbon at steady state for a Ru/TiO$_2$ catalyst is $0.8 \cdot 10^{-7}$ mol, resulting in a coverage of superficial cobalt atoms by active carbon at steady state calculated by us of about 1.5%; the value obtained by Winslow and Bell for the same catalyst (16) is 12%, whereas Mims and McCavendish on a silica supported cobalt catalyst (19) found 18500 mol$_C$/g$_{cat}$ leading to a coverage of superficial Co, from our calculations, of about 17%. Biloen *et al.* (18) also found the carbon coverage to be 4% on the unsupported Co catalyst and 14% on the Ru/γ-Al$_2$O$_3$ catalyst. From inspection of Figure 10, though, it is evident that the coverage of the catalyst by active carbon is not very sensitive to the presence of water. Therefore, a different amount of carbonaceous species on the surface cannot be invoked as an explanation of the lower methane selectivity and higher C$_{5+}$ and olefin selectivity at high water concentration on a Co/SiO$_2$ catalyst at 05MPa and 453 K.

Subsequently carbon coverage measurements were conducted on the Co/TiO$_2$ catalyst at 2.0 MPa and 473 K catalyst, at which conditions the effect of water was observed on both the CO consumption rate and product selectivities. In order to perform a more thorough statistical analysis, repeated measurements were collected at two different space velocities and by adding water at the higher space velocity: the results of these experiments are reported in Table 1.

From those data it is evident that to an increase of the water partial pressure from 0.17 atm to 3.04 atm, at which the rate increases from 1.51 mmol/h/g to 2.83 mmol/h/g and the methane selectivity decreases from 9.1 % to 5.3 %, the active carbon coverage detected by the switch method does not change significantly. The hypothesis that the number of active carbon in the presence of water is greater than in dry conditions was also verified by a statistical test and rejected These results suggest that both the higher activity and the changes in selectivity observed on the Co/TiO$_2$ catalyst cannot be attributed to a significantly greater number of active carbon adsorbed on the surface. The higher rate of CO consumption could hence be explained by hypothesizing a higher reactivity of the same amount of carbonaceous species, which may not be observed by the titration technique here adopted. Indeed, if water played a role in activating the carbon adsorbed on the surface during FTS, a switch to a pure hydrogen stream would not be able to detect it.

Alternatively, since the direct involvement of water into the mechanism of CO consumption was ruled out by the kinetic isotope effect experiments (11), the enhancement of the rate of CO consumption at high water partial pressure could derive from the easier transport of the reactants to the catalytic sites through the liquid waxes filling the pores. This phenomenon might be due to the formation of an aqueous phase, which would facilitate the transport of CO and H$_2$ (5). Assuming a dependence of the CO consumption rate as $r_{CO} = k \cdot p_{H2}^{0.74} p_{CO}^{-0.24}$ (21), an equal increase of the amount of CO and H$_2$ dissolved in the liquid, due to a minor transport limitation of H$_2$ and CO, would positively affect the velocity, whereas the change in the concentration of adsorbed CO with respect to hydrogen could be such as to decrease the methane formation. The fact that the carbon coverage is not greatly affected by the presence of water might be explained if we consider that the amount of adsorbed carbon is much greater than the coverage by hydrogen. Hence, to a decrease of the number of carbon, to which the titration method here used may not be sensible enough, would correspond a significant increase of the adsorbed hydrogen, leading eventually to a higher rate. The lack of effect of water on rate for the silica supported catalyst can also be explained, following Iglesia *et al.* (5), invoking the absence of diffusion limitation of the reactants due to the presence of larger pores, that would require higher H$_2$O concentrations to form a water-rich condensed

phase. Still, further investigations are needed to understand the effect of water on activity and selectivity of cobalt catalysts.

Conclusions

The effect of the partial pressure of water on activity and selectivity of Co-based catalysts was studied. A decrease of methane selectivity and an increase of olefinicity was observed on both the silica and the titania supported catalysts respectively at 0.5 MPa and 453 K, and 2 MPa and 473 K. The Co/TiO_2 catalyst showed also a greater rate of CO consumption at high water partial pressure. The carbon adsorbed on the surface during the reaction was measured by means of hydrogen titration at real Fischer-Tropsch conditions (i.e. high temperature and pressure) on both catalysts. The number of active carbon adsorbed on the catalytic surface was found not be dependent on the partial pressure of water, in the range of operative conditions investigated. Therefore the effects of the partial pressure of water, in particular the increase of the rate of CO consumption, cannot be attributed to a higher coverage of the surface by active carbon. The effect of water could derive either from a higher reactivity of the same number of carbon species, or from the formation of an intrapellet aqueous phase which would enhance the transport of the reactants to the catalytic sites.

References

1. Schanke, D., Hilmen, A. M., Bergene, E., Kinnari, K., Rytter, E., Adnanes, E., and Holmen, A., *Catal. Lett.* 34, 269 (1995).
2. van Berge, P. J., van der Loosdrecht, J., Barradas, S., and van der Kraan, A. M., *Catal. Today.* 58, 321 (2000).
3. Gottschalk, F. M., Copperthwaite, R. G., van der Riet, M., and Hutchings, G. T., *Appl. Catal.* **38**, 103 (1998).
4. Johnson, B. G., Bartholomew, C. H., and Goodman, D. W., *J. Catal.* **128**, 231 (1991).
5. Kim, C. J., U.S. Patent 5,227,407 (1993), assigned to Exxon. Res. Eng. Co.
6. Iglesia, E., *Appl. Catal. A* **161**, 59 (1997).
7. Schulz, H., van Steen, E., and Claeys, M., *Stud. Surf. Sci. Catal.* **81**, 455 (1994).
8. Dry, M. E., *Appl. Catal. A.* **138**, 319 (1996).
9. Adesina, A. A., *Appl. Catal. A.* **138**, 345 (1996).
10. van der Laan, G. P., and Beenackers, A. A. C. M., *Catal. Rev. Sci. Eng.* **41**, 255 (1999).
11. Tu, M., Pinna, D., and Iglesia, E., *manuscript in preparation*.
12. Krishnamoorthy, S., Li, S., Meitzner, G. D., and Iglesia, E., *submitted to Catal. Lett*.
13. Winslow, P., and Bell, A. T., *J. Catal.* **86**, 158 (1984).
14. Bianchi, D., Borcar, S., Teule-Gay, F., and Bennet, C. O., *J. Catal.* **82**, 442 (1983).
15. Bianchi, D., Tau, L. M., Borcar, S., and Bennet, C. O., *J. Catal.* **84**, 358 (1983).
16. Winslow, P., and Bell, A. T., *J. Catal.* **94**, 385 (1985).
17. De Pontes, M., Yokomizo, G. H., and Bell, A. T., *J. Catal.* **104**, 147 (1994).
18. Biloen, P., Helle, J. N., van den Berg, F. G. A., and Sachtler, W. M. H., *J. Catal.* **81**, 450 (1983).
19. Mims, C. A., and McCavendish, L. E., *J. Phys. Chem.* **91**, 929 (1987).
20. Zowtiak, J. M., Weatherbee, G. D., and Bartholomew, C. H., *J. Catal.* **82**, 230 (1983).
21. Zowtiak, J. M., Weatherbee, G. D., and Bartholomew, C. H., *J. Catal.* **83**, 107 (1983).

22.   Zennaro, R., Tagliabue, M., and Bartholomew, C. H., *Catal. Today.* **58**, 309(2000).
23.   Iglesia, E., Reyes, S. C., Madon, R. J., and Soled, S. L., *Advances in Catal.* **39**, 221 (1993).
24.   Reid, R. C., Prausnitz, J. M., and Sherwood, T. K., The Properties of Gases and Liquids, McGraw-Hill, New York, 1977.

Table 1. Results from the experiments on the 15 % Co/TiO$_2$ catalyst at 2.0 MPa, 473K,

H$_2$/CO = 2

	SV = 36.3 min^{-1}		SV = 28.2 min^{-1}		SV = 36.3 min^{-1}	
p$_{H2O}$ (atm)	0.17 ±	0.02	0.20 ±	0.06	3.04	± 0.03
r$_{CO}$ (mmol/h/g)	1.51 ±	0.20	1.35 ±	0.44	2.83	± 0.22
CH$_4$ selectivity (%)	9.11 ±	0.82	8.79 ±	1.27	5.31	± 0.53
C* (μmol)	23.4 ±	3.31	24.8 ±	4.75	25.93	± 5.10

Figure 1. Rate of CO consumption as a function of water partial pressure. (21.9 wt.% Co/SiO_2, P = 0.5 MPa, T = 453 K, H_2/CO = 2).
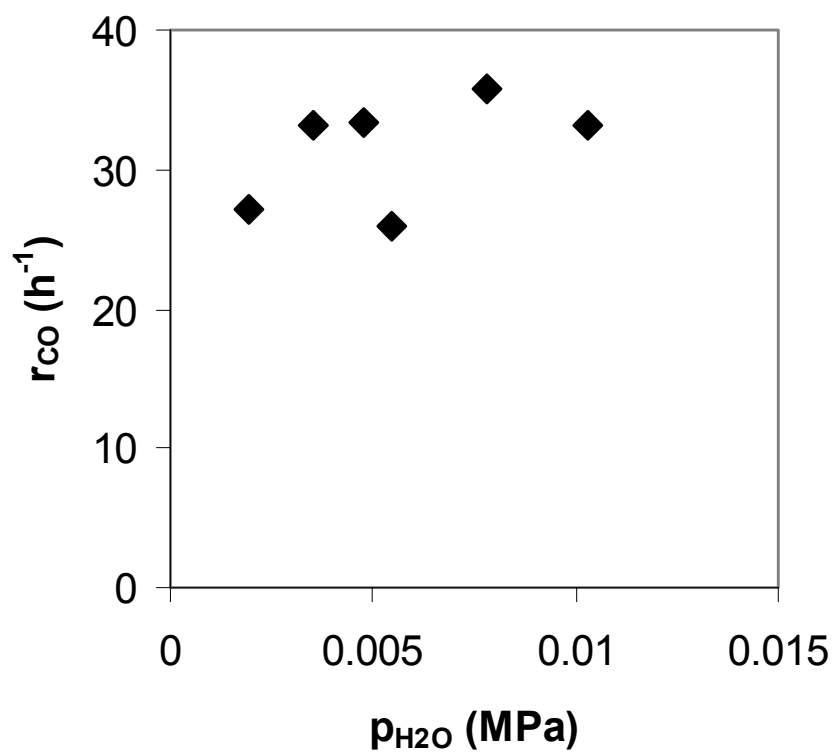
Figure 2. CH$_4$ ($\blacklozenge$) and C$_{5+}$ ($\blacktriangle$) selectivity as a function of water partial pressure. (21.9 wt.% Co/SiO$_2$, P = 0.5 MPa, T = 453 K, H$_2$/CO = 2).
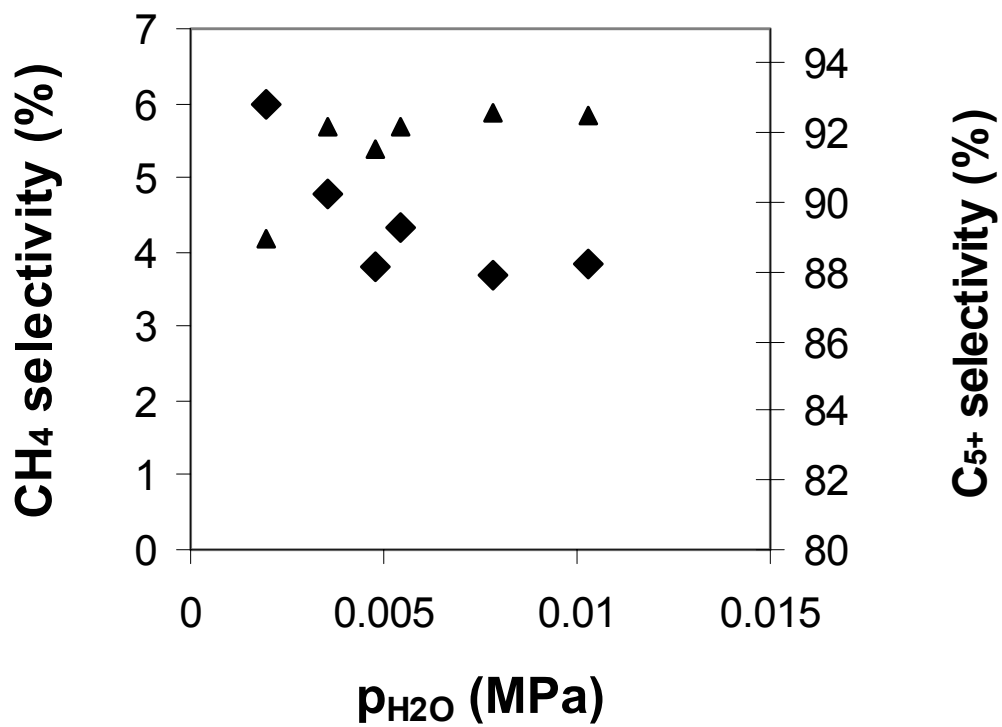
Figure 3. *1*-Pentene/*n*-pentane ratio as a function of water partial pressure. (21.9 wt.% Co/SiO$_2$, P = 0.5 MPa, T = 453 K, H$_2$/CO = 2).
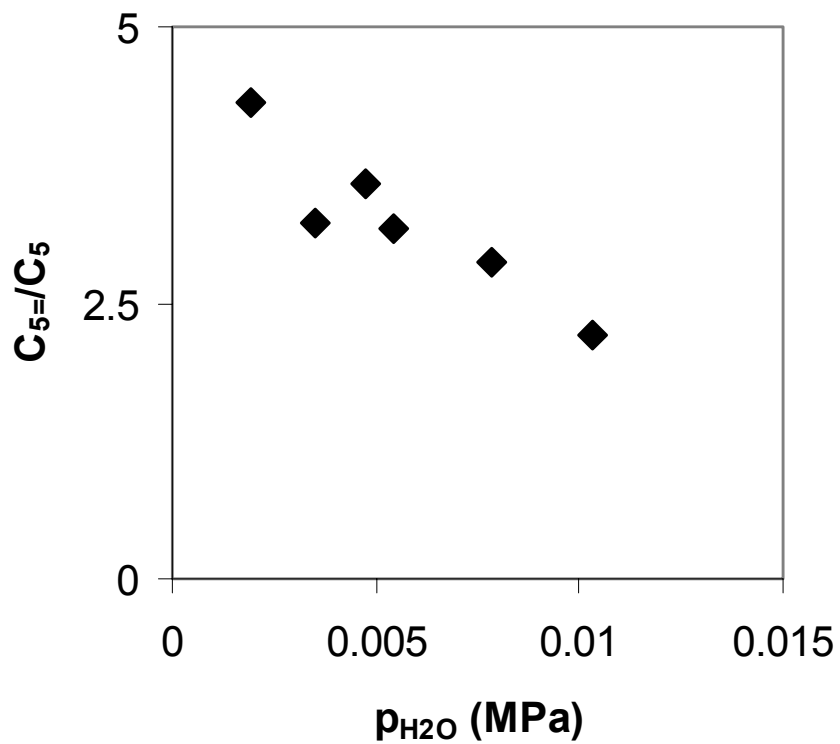
Figure 4. Rate of CO consumption as a function of water partial pressure. Filled symbols: space velocity runs, Open symbols: added water. (15 wt.% Co/TiO_2, P = 2.0 MPa, T = 473 K, H_2/CO = 2).
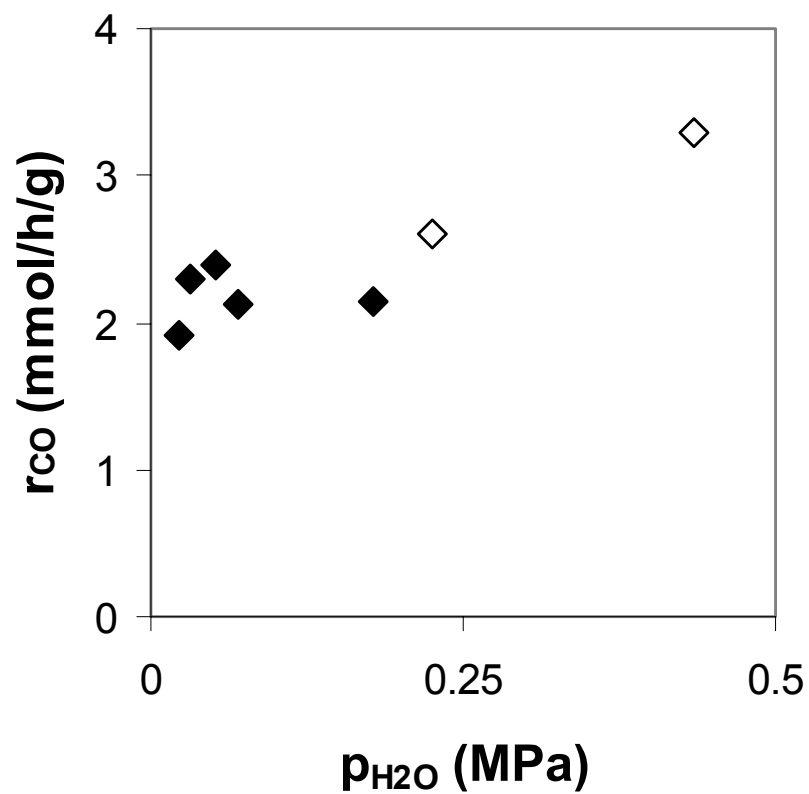
Figure 5. CH$_4$ (◆) and C$_{5+}$ (▲) selectivity as a function of water partial pressure. Filled symbols: space velocity runs, Open symbols: water addition runs. (15 wt.% Co/TiO$_2$, P = 2.0 MPa, T = 473 K, H$_2$/CO = 2).
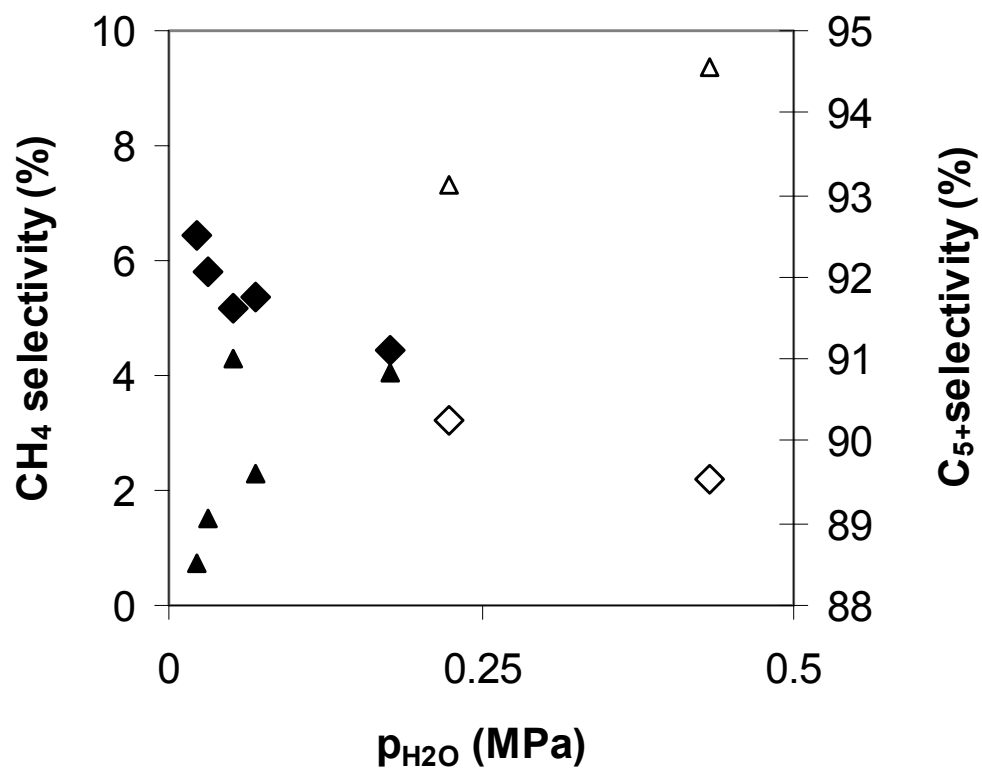
Figure 6. Transient of CO, H_2 and CH_4 flow rates after switch from syngas to methane. (15 wt.% Co/TiO_2, P = 2.0 MPa, T = 473 K, H_2/CO = 2, residence time = 1.7 s, CO conversion = 6.3 %, CH_4 selectivity = 9.6 %).
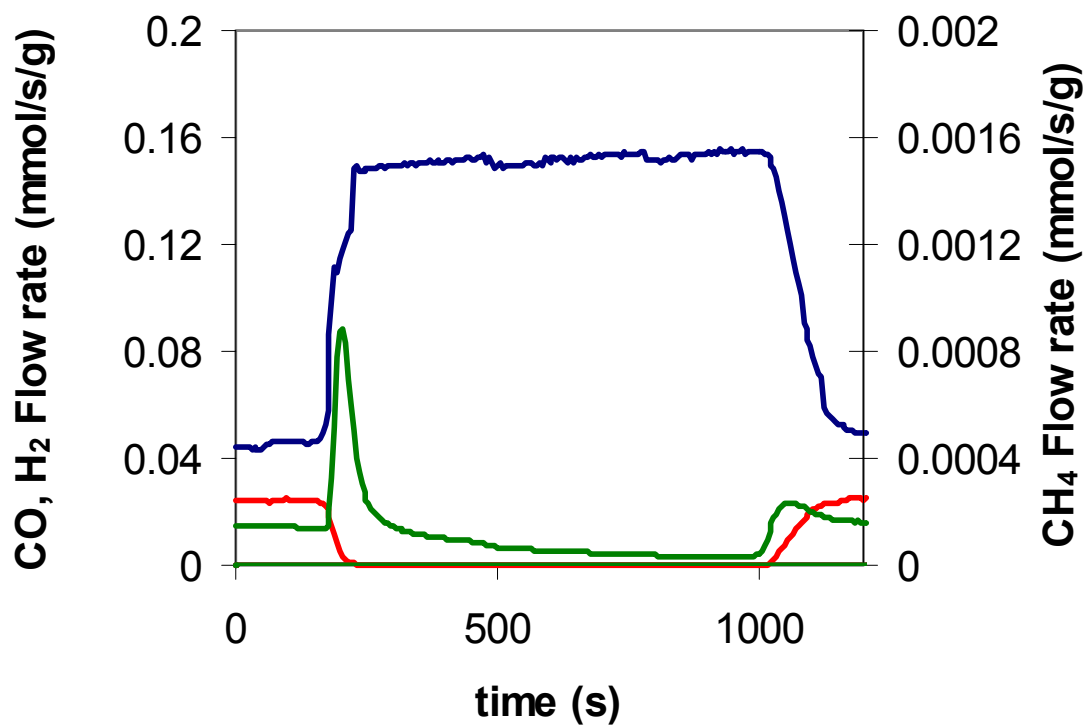
Figure 7. Transient of Ar flow rate after switch from syngas to methane. ($\blacklozenge$) experimental, line$-$ model . (15 wt. % Co/TiO_2, P = 2.0 MPa, T = 473 K, H_2/CO = 2, residence time = 1.7 s, CO conversion = 6.3 %, CH_4 selectivity = 9.6 %).
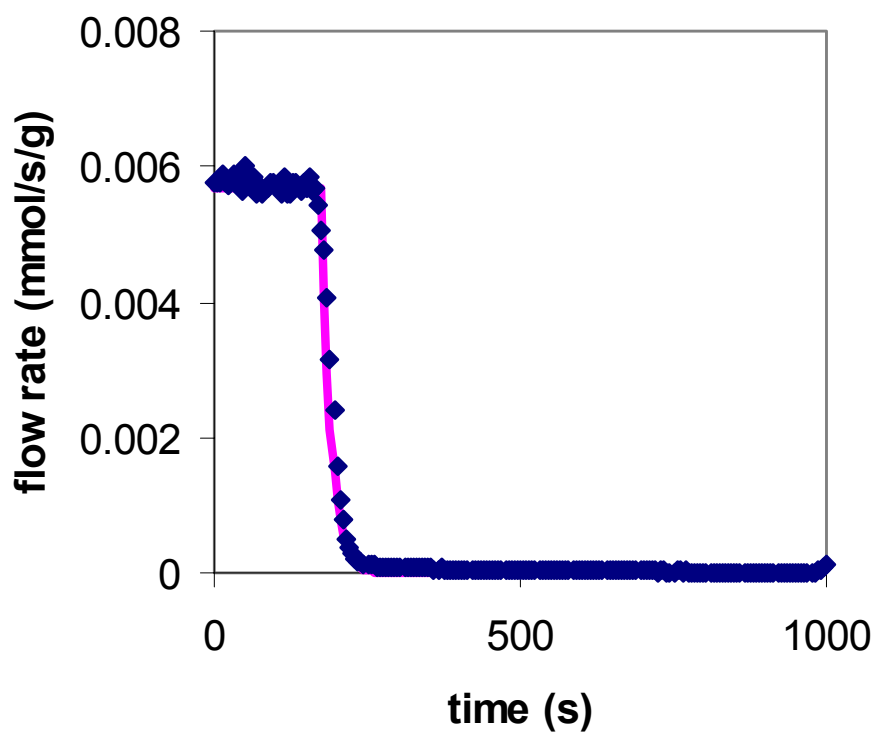
Figure 8. Normalized flow rate of CH_4 after switch from syngas to methane. (15 wt.% Co/TiO_2, P = 2.0 MPa, T = 473 K, H_2/CO = 2, residence time = 1.7 s, CO conversion = 6.3 %, CH_4 selectivity = 9.6 %).
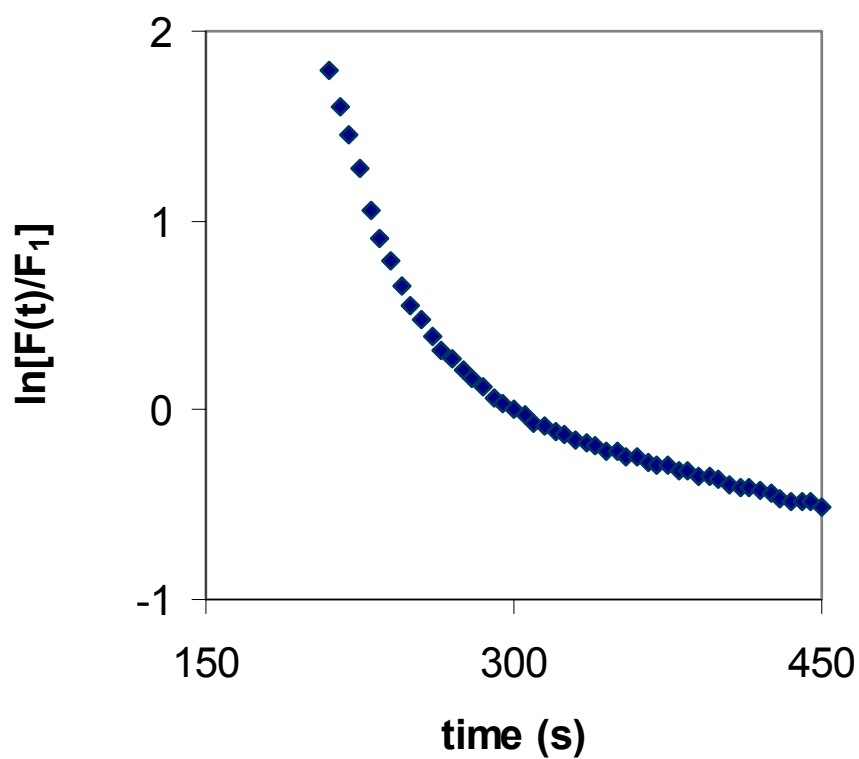
Figure 9. Flow rate of CH_4 after switch from syngas to methane. (◆) experimental, line –
model (15 wt.% Co/TiO_2, P = 2.0 MPa, T = 473 K, H_2/CO = 2, residence time = 1.7 s, CO
conversion = 6.3 %, CH_4 selectivity = 9.6 %).
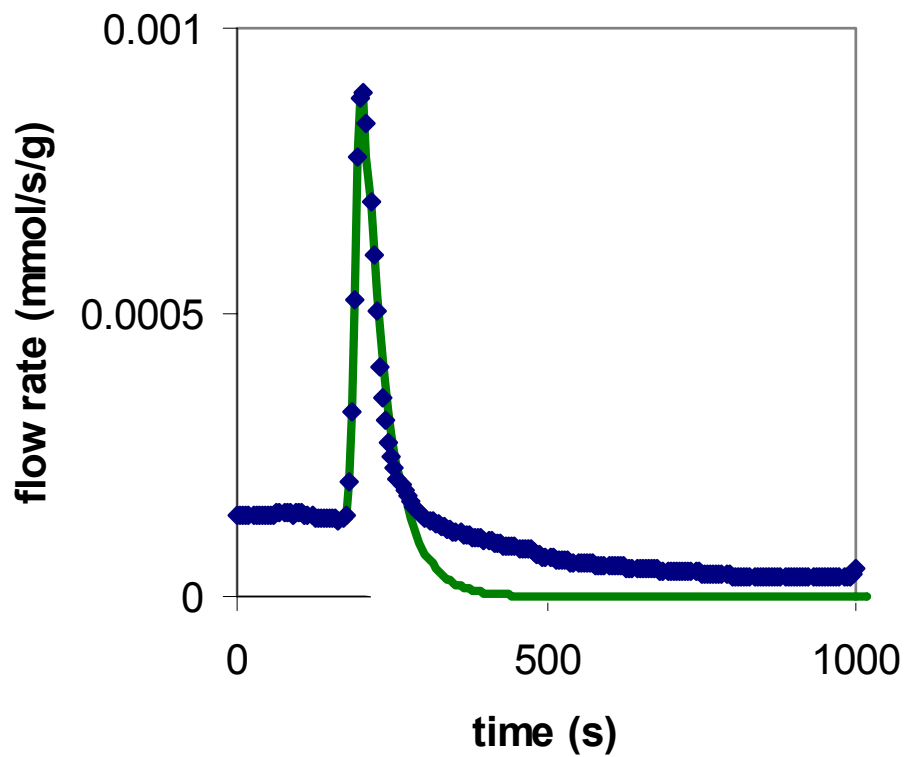
Figure 10 – Carbon coverage as a function of water partial pressure. (21.9 wt.% Co/SiO_2, P = 0.5 MPa, T = 453 K, H_2/CO = 2).
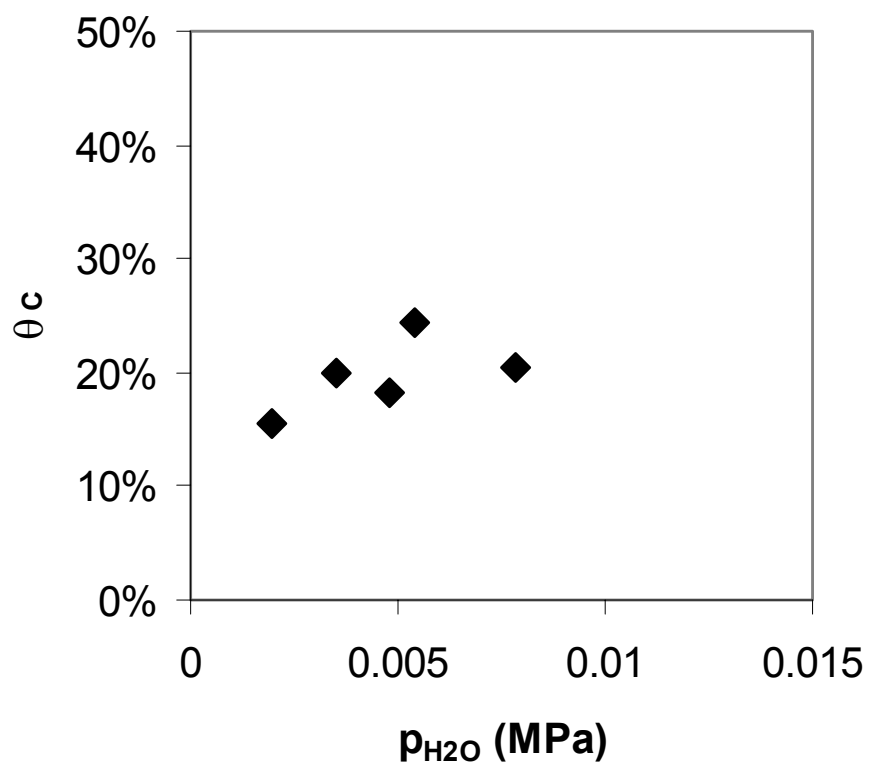
Task 12. Reporting/Project Management

Three monthly and one quarterly reports have been completed.